European Journal of Medicinal Chemistry 218 (2021) 113391

Contents lists available at ScienceDirect

European Journal of Medicinal Chemistry

journal homepage: http://www.elsevier.com/locate/ejmech

Discovery of a potent, highly selective, and orally bioavailable inhibitor of CDK8 through a structure-based optimisation

Mingfeng Yu, Yi Long, Yuchao Yang, Manjun Li, Theodosia Teo, Benjamin Noll, Stephen Philip, Shudong Wang*

Drug Discovery and Development, Cancer Research Institute, Clinical and Health Sciences, University of South Australia, Adelaide, South Australia, 5000, Australia

ARTICLE INFO

Article history:
Received 16 February 2021
Received in revised form
16 March 2021
Accepted 17 March 2021
Available online 26 March 2021

Keywords:
CDK8 inhibitor
Structure-based optimisation
Kinase selectivity
Oral bioavailability
Anti-proliferation mechanism
MV4-11

ABSTRACT

CDK8 is deregulated in multiple types of human cancer and is viewed as a therapeutic target for the treatment of the disease. Accordingly, the search for small-molecule inhibitors of CDK8 is being intensified. Capitalising on our initial discovery of AU1-100, a potent CDK8 inhibitor yet with a limited degree of kinase selectivity, a structure-based optimisation was carried out, with a series of new multi-substituted pyridines rationally designed, chemically prepared and biologically evaluated. Such endeavour has culminated in the identification of **42**, a more potent CDK8 inhibitor with superior kinomic selectivity and oral bioavailability. The mechanism underlying the anti-proliferative effect of **42** on MV4-11 cells was studied, revealing that the compound arrested the G1 cell cycle and triggered apoptosis. The low risk of hepato- and cardio-toxicity of **42** was estimated. These findings merit further investigation of **42** as a targeted cancer therapeutic.

1. Introduction

As a member of the cyclin-dependent kinase (CDK) family, CDK8 is typically involved in regulating transcription in two forms [1,2]: (i) partnered with cyclin C, CDK8 phosphorylates a number of transcription factors such as signal transducer and activator of transcription 1 (STAT1) [3], neurogenic locus notch homolog proteins (NOTCH) [4] and mothers against decapentaplegic homologs (SMADs) [5], modulating their activity or priming them for ubiquitin-mediated proteasomal degradation; or (ii) recruited to form a four-subunit kinase module that additionally consists of cyclin C, MED12 and MED13, CDK8 binds reversibly to the Mediator complex, a central integrator as well as a signal processor and transducer in the RNA polymerase II general transcriptional machinery [6–8]. In contrast to the well-studied role of CDK8 in controlling gene expression, its function in cell division remains much less understood [9], with related studies reported sporadically [10,11]. For instance, the Skp2-MacroH2A1-CDK8 axis has been demonstrated to orchestrate the G2/M transition in mouse embryonic fibroblasts [11].

Deregulation of CDK8 has been considered as a driver lesion in various types of human cancer. Specifically, *CDK8* was identified as an oncogene in colorectal cancer [12], and amplification and/or mutation of this gene were detected in melanoma [13], acute myeloid leukaemia (AML) [14], and cancers of breast [11], pancreas [15], prostate [16], gastrointestinal tract, bladder, and other organs [17]. Silencing the expression of *CDK8* with microRNAs, small interfering RNAs or short hairpin RNAs inhibited *in vitro* cell proliferation of breast [18–20], prostate [16], colorectal [12,21] and pancreatic [15] cancers, and melanoma [13]. Correspondingly, pharmacological suppression of the kinase activity of CDK8 by exogenous small-molecule inhibitors shrank tumours not only in xenograft models derived from cell lines of COLO205, HCT116, LS513, LS1034 and SW620 colorectal [22–25], MCF7 and MDA-MB-231 breast [26,27], and VCaP prostate [10] cancers, SET-2, KG-1 and MV4-11 AML [14,28], and RPMI 8226 myeloma [29,30], but also in patient-derived xenografts [24]. In addition, treatment of natural killer cells with CDK8 inhibitors has been very recently found to enhance the lysis of HL-60 AML cells and B-chronic lymphocytic leukaemia cells *in vitro*, and to promote tumour surveillance in the murine B16–F10-luc2 syngeneic melanoma model [31]. Taken together, CDK8 represents a therapeutic target for validation,

* Corresponding author.
E-mail address: shudong.wang@unisa.edu.au (S. Wang).

https://doi.org/10.1016/j.ejmech.2021.113391
0223-5234/

particularly in the treatment of human cancer, and consequently exogenous small-molecule inhibitors of this kinase with adequate potency, selectivity and drug-like properties are highly sought-after.

The initial discovery of some CDK8 inhibitors (Fig. 1) arose serendipitously from the searches for inhibitors of alternative targets. Typical examples include (i) cortistatin A, a natural product with anti-angiogenic activity [32,33]; (ii) senexin A, which was developed based upon the results of a high-throughput screening of more than 100,000 commercially available small molecules for the inhibition of p21-induced transcription [34,35]; and (iii) CCT251545 that was originally identified as an inhibitor of the WNT signalling pathway from a high-throughput cell-based reporter assay [25,36]. While structurally simpler steroidal inhibitors and degraders of CDK8 were derived from cortistatin A using analogue-based drug design [37,38], medicinal chemistry optimisation of senexin A and CCT251545 gave rise to senexin B (also known as BCD-115) [39] and CCT251921 [23], respectively, with improved CDK8 inhibitory activity and specificity. Among them, BCD-115 has been clinically trialled in combination with endocrine therapy in women with estrogen receptor-positive/human epidermal growth factor receptor 2-negative, locally advanced and metastatic breast cancer (NCT03065010: phase I completed). The other CDK8 inhibitor that has entered a clinical trial is SEL120 (reported as SEL120-34A in the literature [28]) for treating AML or high-risk myelodysplastic syndrome (NCT04021368: phase I ongoing). Alternative CDK8 inhibitors with diverse chemical scaffolds have been recently reviewed [2,40–42].

We have ongoing interests in discovering and developing small-molecule inhibitors of CDKs for cancer therapy [43–56], with our recent attention turned to a hunt for potent and selective CDK8 inhibitors with favourable drug-like properties [2,57,58]. One of our attempts has resulted in the identification of AU1-100 (Fig. 1) as a potent CDK8 inhibitor [58]. However, AU1-100 displayed a moderate inhibitory specificity for CDK8 in a screening against a selection of 62 kinases, with the kinase activity of GSK-3α/β suppressed to the same magnitude as that of CDK8 (*i.e.*, $K_i = 0.014$, 0.013 and 0.004 μM for CDK8, GSK-3α and GSK-3β, respectively), hampering the understanding of underlying mechanisms of its anti-proliferative effect on MV4-11 cells and its toxicity towards murine long bones and lungs. Besides, the *in vitro* drug metabolism and pharmacokinetics (DMPK) profile of AU1-100 was suboptimal. For instance, the compound inhibited two cytochrome P450 (CYP450) enzymes moderately, increasing the likelihood of inducing drug-drug interactions in combination therapy. Herein we describe our endeavour in the structure-based optimisation of AU1-100 for superior CDK8 inhibitory selectivity and drug-like properties.

2. Results and discussion

2.1. Structure-based design

To increase the kinase inhibitory selectivity for CDK8 over GSK-3α/β requires, as a first step, a comprehension of the molecular basis for the potency of AU1-100 towards the three kinases. The compound was first docked into one of CDK8 crystal structures (PDB ID: 5BNJ) using Glide, a rapid and accurate approach for the ligand-receptor docking and the scoring of ligand poses [59,60]. The binding mode thus generated predicts multiple interactions of AU1-100 with CDK8, which include, but are not limited to, hydrogen bonds, π-cation stacking and Cl-π contact (Fig. 2). Intriguingly, the π-cation stacking engages the furan component only—rather than the entire benzofuranyl moiety—in interacting with CDK8-R356. A similar interaction was postulated as a contributor of the exquisite selectivity of CCT251545 for CDK8 due to an uncommon insertion of C-terminal R356 into the hinge region of the kinase [36]. Accordingly, we envisaged that replacement of the benzofuranyl moiety with a smaller five-membered aromatic ring at the pyridine-C5 position could hold promise of fine-tuning the degree of CDK8 inhibitory selectivity (Fig. 3).

At the same time, our structural analysis of known CDK8 inhibitors derived from a pyridine core revealed that both *ortho* positions of the pyridine ring were scarcely exploited, with very few examples demonstrated [23,30,61]. Among them is CCT251921 with a primary amino group at the pyridine-C2 position (Fig. 1);

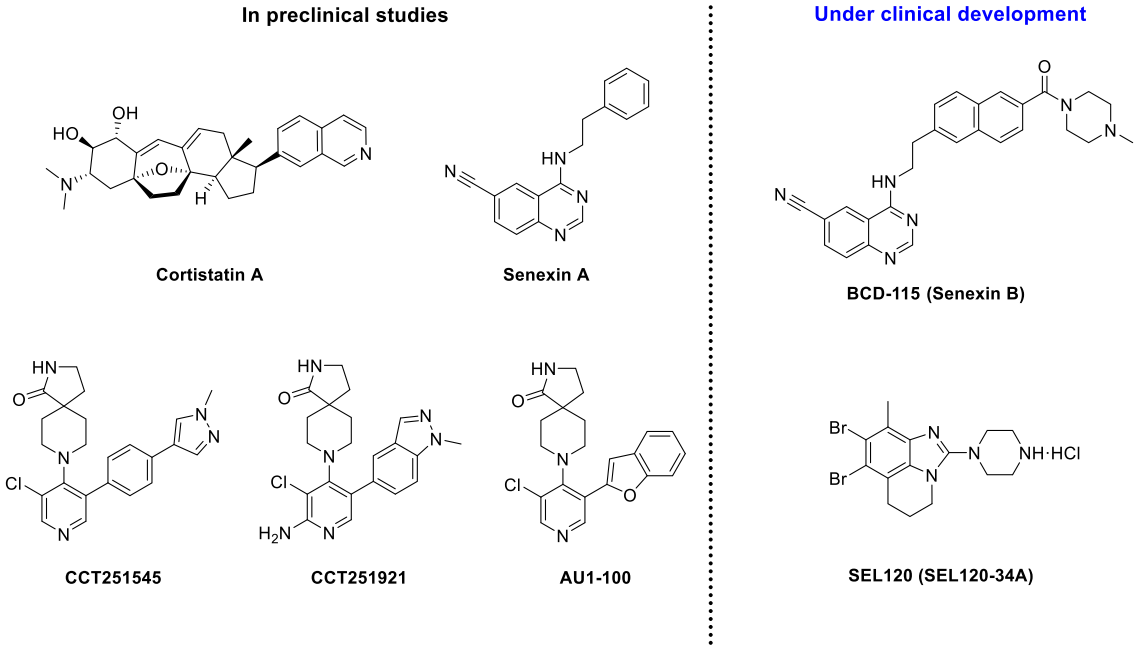

Fig. 1. Chemical structures of selected CDK8 inhibitors.

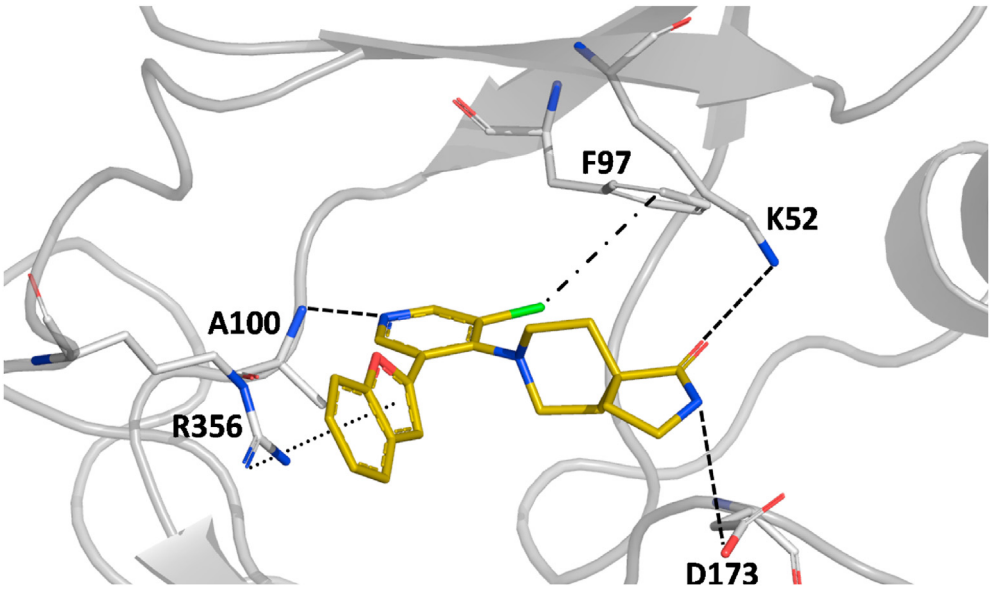

Fig. 2. Predicted binding pose of AU1-100 (in gold sticks) in CDK8/cyclin C (in grey ribbons, with selected amino acid residues annotated). Hydrogen bonds are drawn as dashed lines, and π-cation and Cl-π interactions as dotted and dash-dotted lines, respectively. Nitrogen atoms are shown in blue, oxygen atoms in red, and the chlorine atom is coloured green. The illustration was generated using PyMOL Molecular Graphics System Version 2.4.0 Schrödinger, LLC.

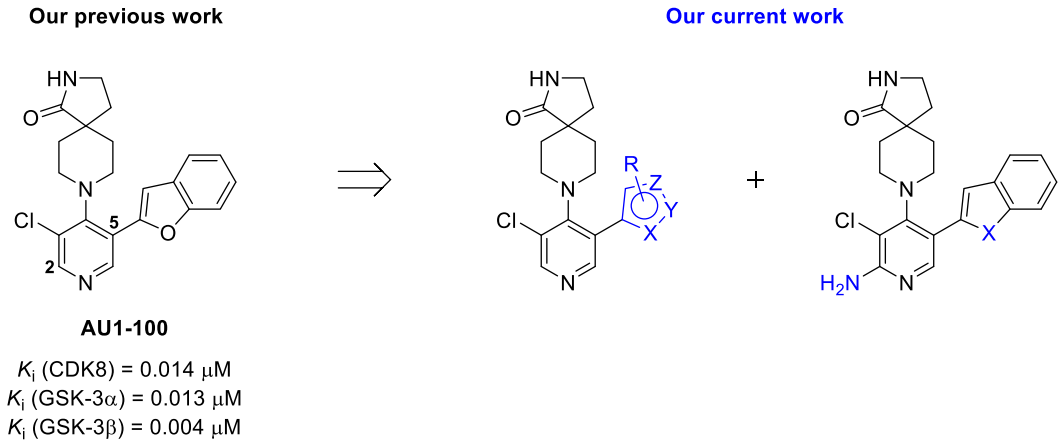

Fig. 3. Design of novel CDK8 inhibitors.

this amino group was found to form a hydrogen bond with the backbone carbonyl of CDK8-D98, contributing to the affinity for the kinase [23]. The counterpart of CDK8-D98 in GSK-3α is E196 that contains one more carbon atom in the side chain [62]. This residue difference led us to wonder whether introduction of an appropriate-size hydrogen bond donor onto the pyridine-C2 position of AU1-100 would perturb the interaction with GSK-3α but maintain or even strengthen the contact with CDK8. Such molecules as a 2-amino derivative of AU1-100 could be docked into a GSK-3α crystal structure to test our hypothesis, but regrettably no crystal structure of this kinase was (and is) available in the Protein Data Bank. Nevertheless, prototype molecules with a 2-aminopyridine scaffold were pursued to examine the hypothesis experimentally (Fig. 3).

2.2. Synthesis

Preparation of 8-(3-chloro-5-aryl-pyridin-4-yl)-2,8-diazaspiro[4.5]decan-1-ones **4**–**32** was accomplished using our previously reported synthetic route [58]. Briefly, 3-bromo-5-chloropyridine **1** sequentially underwent (i) lithium-assisted chlorination with hexachloroethane at the C4 position, (ii) nucleophilic aromatic displacement of the newly introduced chlorine by *tert*-butyl 1-oxo-2,8-diazaspiro[4.5]decane-8-carboxylate, and (iii) Pd(dppf)$Cl_2 \cdot CH_2Cl_2$-catalysed Suzuki coupling at the C5 position with boronic acids or boronate esters of diverse five-membered heteroaromatic rings, giving rise to the desired compounds **4**–**32** in varying yields (Scheme 1).

Synthesis of 8-(2-amino-5-(benzofuran/benzothiophen-2-yl)-3-chloropyridin-4-yl)-2,8-diazaspiro[4.5]decan-1-ones **42** and **43** was carried out *via* multiple steps (Scheme 2). Detailedly, 4-chloropyridin-2-amine **33** was successively halogenated at C5 and C3 positions with *N*-bromosuccinimide (NBS) at room temperature and with *N*-chlorosuccinimide (NCS) at reflux, respectively, affording 5-bromo-3,4-dichloropyridin-2-amine **35** in an overall yield of approximately 56%. To minimise the chance of the 2-amino group interfering with the subsequent nucleophilic aromatic substitution and palladium-catalysed cross-coupling reaction, **35** was

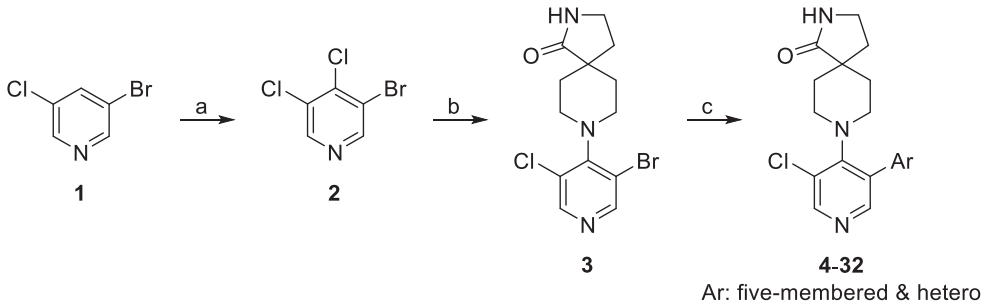

Scheme 1. Synthesis of 8-(3-chloro-5-aryl-pyridin-4-yl)-2,8-diazaspiro[4.5]decan-1-ones **4**–**32**. *Reagents and conditions*: (a) lithium diisopropylamide (2.0 M in THF/heptane/ethylbenzene), hexachloroethane, THF, −78 °C, 2 h, 65%; (b) *tert*-butyl 1-oxo-2,8-diazaspiro[4.5]decane-8-carboxylate, triethylamine, 1-methoxy-2-propanol, microwave 150–300 W, 220 °C, 2.5 h, 79%; (c) appropriate boronic acid or boronate ester, Pd(dppf)$Cl_2 \cdot CH_2Cl_2$, 0.5 M Na_2CO_3, CH_3CN, microwave 150–300 W, 120–160 °C, 1–2 h, 10–67%.

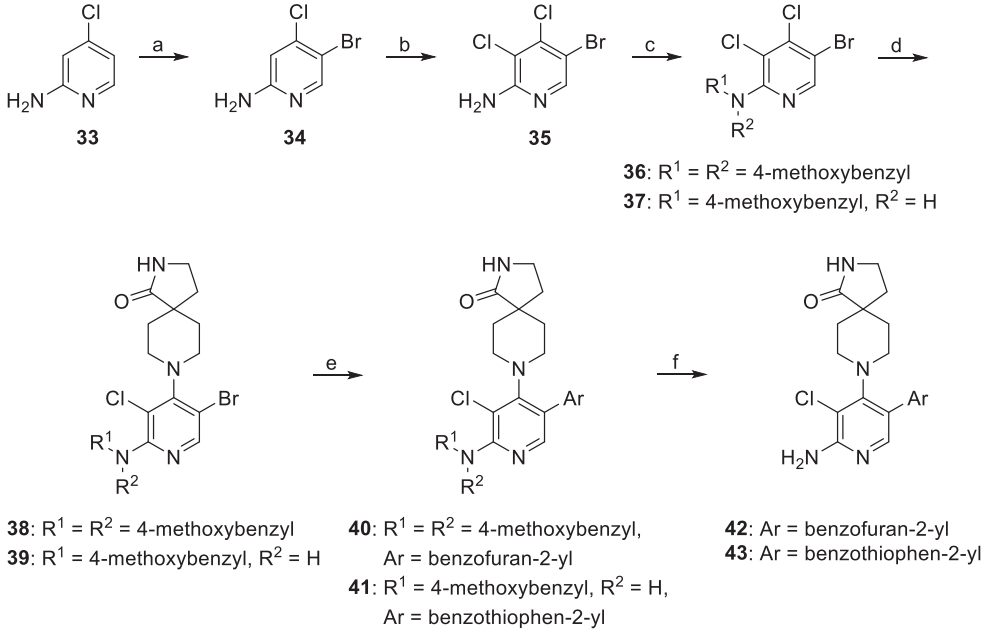

Scheme 2. Synthesis of 8-(2-amino-5-(benzofuran/benzothiophen -2-yl)-3-chloropyridin-4-yl)-2,8-diazaspiro[4.5]decan-1-ones **42** and **43**. *Reagents and conditions*: (a) NBS, CH_3CN, rt, 3 h, 58%; (b) NCS, CH_3CN, reflux, 3 h, 96%; (c) sodium hydride (60% dispersion in mineral oil), 4-methoxybenzyl chloride, DMF, 0 °C to rt, 2.25 h, **36**: 66%, **37**: 28%; (d) *tert*-butyl 1-oxo-2,8-diazaspiro[4.5]decane-8-carboxylate, KF, triethylamine, *N*-methyl-2-pyrrolidone, microwave 150–300 W, **38**: 220 °C, 1 h, 48%, **39**: 225 °C, 2.5 h, 68%; (e) 2-(benzofuran-2-yl)-4,4,5,5-tetramethyl-1,3,2-dioxaborolane or benzo[*b*]thiophen-2-ylboronic acid, Pd(dppf)$Cl_2 \cdot CH_2Cl_2$, 0.5 M Na_2CO_3, CH_3CN, microwave 150–300 W, 130 °C, 1 h, **40**: 44%, **41**: 45%; (f) TFA, rt, o/n, **42**: 75%, **43**: 61%.

protected by 4-methoxybenzyl to give both mono- and di-substituted forms in an excellent overall yield (94%), with the latter being the major product (**36**: 66%). Fully and partially protected forms **36** and **37** were individually subjected to microwave-assisted nucleophilic aromatic displacement of the chlorine at the C4 position with *tert*-butyl 1-oxo-2,8-diazaspiro[4.5]decane-8-carboxylate at very high temperature (220–225 °C); potassium fluoride (KF) was used to facilitate the displacement *via* the *hal*ide *ex*change (Halex) process (*i.e.*, conversion of 4-Cl to 4-F that served as a better leaving group) [63]. Compounds **38** and **39** thus obtained were coupled with their respective 2-(benzofuran-2-yl)-4,4,5,5-tetramethyl-1,3,2-dioxaborolane and benzo[*b*]thiophen-2-ylboronic acid in the presence of Pd(dppf)$Cl_2 \cdot CH_2Cl_2$, yielding the corresponding adducts **40** and **41** in decent yields (**40**: 44% and **41**: 45%). Removal of the 4-methoxybenzyl protecting group(s) from each adduct was effected in trifluoroacetic acid (TFA) at room temperature overnight, furnishing **42** and **43** in yields of 75% and 61%, respectively.

2.3. Structure–activity relationship analysis

Our previous studies showed that MV4-11 AML cells were the most sensitive to AU1-100 in a screening against a panel of 19 human cancer cell lines with different origins [58]. Accordingly, this cell line was chosen to assess the anti-proliferative effect of the newly synthesised compounds using our in-house resazurin assay [64]. In parallel, the inhibitory activity of these compounds towards CDK8/cyclin C was evaluated externally with the ^{33}PanQinase® activity assay—a radiometric kinase assay using [γ-^{33}P]-ATP.

As described in Section 2.1, docking results showed that only the furan component of AU1-100 was projected to be involved in the π-cation interaction with the positively charged guanidinium side chain of CDK8-R356 (Fig. 2). To confirm this experimentally, **4** with a simpler furan-2-yl substituent at the pyridine-C5 position was first synthesised and tested (Table 1). This compound was just slightly less active towards both CDK8 and MV4-11 cells when compared with its benzofuran-2-yl counterpart AU1-100

Table 1
Chemical structures and biological activities of **4**–**8**.

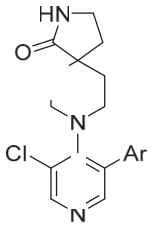

4–**8**

Compound	Ar	CDK8/cyclin C inhibition, K_i (μM)[a]	MV4-11 anti-proliferation, GI_{50} (μM)[b]
AU1-100 (**38**[c])	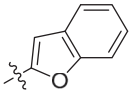	0.014	0.36 ± 0.35
4		0.026	0.94 ± 0.04
40[c]	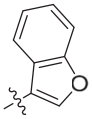	0.048	29.16 ± 1.19
5		0.042	0.75 ± 0.02
39[c]	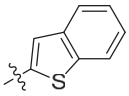	0.014	0.58 ± 0.14
6		0.010	0.48 ± 0.08
41[c]	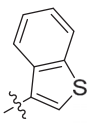	0.021	0.35 ± 0.22

(*continued on next page*)

Table 1 (*continued*)

Compound	Ar	CDK8/cyclin C inhibition, K_i (μM)[a]	MV4-11 anti-proliferation, GI_{50} (μM)[b]
7		0.018	0.19 ± 0.09
35[c]	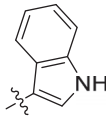	0.056	8.77 ± 2.04
8	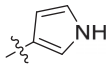	0.014	1.05 ± 0.67

[a] Inhibition of CDK8/cyclin C was measured with the ^{33}PanQinase® activity assay at ProQinase GmbH, and the K_m value used as the ATP concentration. Each apparent inhibition constant (K_i) was calculated using its corresponding IC_{50} value and the K_m (ATP) value.
[b] GI_{50} values were determined in-house by the 72 h resazurin assay, and are presented as mean ± standard deviation derived from at least two replicates.
[c] Compounds and their biological data were previously reported in Ref. [58].

(K_i = 0.014 μM and GI_{50} = 0.36 μM), and maintained low double-digit nanomolar kinase inhibition (K_i = 0.026 μM) and sub-micromolar anti-proliferation (GI_{50} = 0.94 μM). Encouraged by these data, compounds **5**–**8** with a furan-3-yl, a thiophen-2-yl, a thiophen-3-yl and an 1*H*-pyrrol-3-yl, respectively, were further prepared. All four compounds displayed higher inhibitory activities against both CDK8 and MV4-11 cells than did their corresponding benzo-fused counterparts 40, 39, 41 and 35 (reported previously [58]), with K_i and GI_{50} values in ranges of 0.010–0.042 and 0.19–1.05 μM, respectively. Collectively, both enzymatic and cellular inhibitory activities of **5**–**8** were comparable, if not superior, to those of AU1-100. These results indicated that replacement of [5,6]-fused aromatic moieties with their constitutive five-membered rings was well tolerated at the pyridine-C5 position.

Given that all the five-membered aromatic rings introduced thus far were not substituted elsewhere, it was deemed advisable to functionalise them to explore the structure–activity relationship further (Tables 2 and 3). Introduction of a small-size methyl (**9**) or a long, linear (ethoxymethoxy)methyl (**11**) onto the furan-2-yl-C5 position of **4** (K_i = 0.026 μM) maintained the potency against CDK8 (**9**: K_i = 0.022 μM and **11**: K_i = 0.036 μM), whereas incorporation of a formyl at the same site reduced CDK8 inhibitory activity by over three times (K_i = 0.082 μM) (Table 2). A similar phenomenon was observed in functionalisation of the thiophen-2-yl ring of **6**. Substitution with a methyl at any available position or with a chlorine atom at C5 caused the inhibition of CDK8 to a degree comparable to that of the parent molecule (**12**–**15**: K_i = 0.008–0.014 μM versus **6**: K_i = 0.010 μM). In contrast, **16** and **17** appended with a 5-acetyl and a 5-formyl, respectively, were more than six-fold less active against the kinase (**16**: K_i = 0.066 μM and **17**: K_i = 0.067 μM). Di-substitution with a 4-methyl and a 5-formyl significantly weakened the CDK8 inhibition, with the K_i value being one order of magnitude higher (**18**: K_i = 0.119 μM). These data suggested that electron-donating groups like methyl and chlorine were tolerated but electron-withdrawing groups such as formyl and acetyl engendered detrimental effects. This postulation was not unexpected because these substituted five-membered aromatic rings were likely to be engaged in the π-cation interaction with CDK8-R356, where electronic properties of their substituents could influence the strength of electrostatic attraction [65]. While the second half of the postulation was confirmed by introduction of a formyl or an acetyl group onto the furan-3-yl ring of **5** or the thiophen-3-yl ring of **7** (Table 3), the first half further tested by attaching an electron-donating phenyl to the furan-2-yl-C5 position of **6** (Table 2). This sizeable attachment gave rise to single-digit nanomolar CDK8 inhibition (**19**: K_i = 0.005 μM), which stimulated the pursuit of bulky pedants at the same position. However, replacement of the phenyl with several azacycle-containing groups including 5-(pyrrolidin-1-ylmethyl) (**20**), 5-(piperidin-1-ylmethyl) (**21**), 5-morpholinomethyl (**22**), 5-((4-Boc-piperazin-1-yl)methyl) (**23**) enfeebled the kinase inhibitory activity by up to 26.4-fold (K_i = 0.032–0.132 μM).

As expected, all the compounds with a formyl or an acetyl substituent at the furan-3-yl or thiophen-3-yl ring were much less potent against CDK8 than their respective parent molecules (**25**: K_i = 0.185 μM versus **5**: K_i = 0.042 μM; **26**–**29**: K_i = 0.052–4.655 μM versus **7**: K_i = 0.018 μM) (Table 3). The 1*H*-pyrrol-3-yl counterpart of furan-3-yl **5** or thiophen-3-yl **7** was a more active inhibitor of CDK8 (**8**: K_i = 0.014 μM), but their 1*H*-pyrazol-4-yl equivalent was far inferior (**30**: K_i = 0.254 μM). Masking the NH site of the latter with a methyl or a difluoromethyl partly restored kinase inhibitory potency (**31**: K_i = 0.230 μM and **32**: K_i = 0.093 μM). Contrastingly, **24** with its pyrrol-2-yl-NH covered by a methyl retained CDK8 inhibitory activity, with a K_i value of 0.030 μM (Table 2).

In general, compounds with their five-membered aromatic rings unsubstituted elsewhere or substituted by electron-donating groups were typically one-digit or low two-digit nanomolar inhibitors of CDK8 (*i.e.*, K_i = 0.005–0.042 μM). Such kinase inhibition was translated into sub-micromolar anti-proliferative effect on MV4-11 cells (GI_{50} = 0.19–0.96 μM) (Tables 2 and 3) with a very few exceptions—**8**, **9** and **11** with K_i values of <0.050 μM yet with GI_{50} values of >1 μM.

Among all the compounds synthesised thus far (Tables 1–3), **19** with a 5-(5-phenylthiophen-2-yl) arm displayed the highest inhibitory potency against CDK8, and therefore was subjected to a screening against a selection of five kinases, namely glycogen synthase kinase (GSK)-3α, GSK-3β, protein kinase C (PKC)-θ, CDK1/cyclin B and CDK9/cyclin T1, all of which were identified as off-targets of AU1-100 [58]. Upon treatment with **19** at a concentration of 1 μM, kinase activities of CDK1/9 and PKC-θ were either hardly affected or slightly diminished, whereas GSK-3α/β deprived

Table 2
Chemical structures and biological activities of **4**, **6** and **9**–**24**.

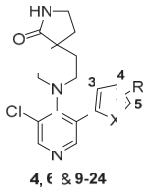

4, **6** & **9-24**

Compound	X	R	CDK8/cyclin C inhibition, K_i (μM)[a]	MV4-11 anti-proliferation, GI_{50} (μM)[b]
4	O	–	0.026	0.94 ± 0.04
9	O	5-CH_3	0.022	4.95 ± 5.07
10	O	5-CHO	0.082	5.19 ± 0.06
11	O	5-$(CH_2O)_2CH_2CH_3$	0.036	2.97 ± 0.38
6	S	–	0.010	0.48 ± 0.08
12	S	3-CH_3	0.008	0.91 ± 0.01
13	S	4-CH_3	0.010	0.65 ± 0.13
14	S	5-CH_3	0.010	0.65 ± 0.08
15	S	5-Cl	0.014	0.56 ± 0.10
16	S	5-$COCH_3$	0.066	1.44 ± 0.67
17	S	5-CHO	0.067	0.75 ± 0.08
18	S	4-CH_3-5-CHO	0.119	2.53 ± 0.13
19	S	5-phenyl	0.005	0.96 ± 0.05
20	S	5-(pyrrolidin-1-ylmethyl)	0.132	3.37 ± 2.25
21	S	5-(piperidin-1-ylmethyl)	0.106	4.01 ± 0.84
22	S	5-morpholinomethyl	0.032	2.96 ± 2.86
23	S	5-((4-Boc-piperazin-1-yl)methyl)	0.046	5.15 ± 0.38
24	NCH_3	–	0.030	0.90 ± 0.06

[a] Inhibition of CDK8/cyclin C was measured with the ^{33}PanQinase® activity assay at ProQinase GmbH, and the K_m value used as the ATP concentration. Each apparent inhibition constant (K_i) was calculated using its corresponding IC_{50} value and the K_m (ATP) value.
[b] GI_{50} values were determined in-house by the 72 h resazurin assay, and are presented as mean ± standard deviation derived from at least two replicates.

of 62% and 74% kinase activity, respectively (Fig. 4). Both percentage values were similar to those of AU1-100, indicating the comparable potency of **19** against both GSK-3 isoforms to that of the control.

Given that the structural diversification at the pyridine-C5 position failed to return an improved inhibitory specificity for CDK8 over GSK-3α/β, the effort was subsequently switched to the modification of the underexplored C2 site. Compounds **42** and **43** with a common 2-amino group were then prepared and evaluated. Both were more effective in inhibiting the kinase activity of CDK8 than their 2-unsubstituted counterparts AU1-100 and 39 (reported previously [58]), with K_i values of 0.009 and 0.007 μM for **42** and **43**, respectively (Table 4). These single-digit nanomolar inhibitory activities towards CDK8 correlated with low sub-micromolar antiproliferative effects on MV4-11 cells (**42**: GI_{50} = 0.60 μM and **43**: GI_{50} = 0.16 μM). In comparison with CCT251921, **42** and **43** were more potent antagonists of CDK8 but weaker inhibitors of MV4-11 cells. Compound **42** was further tested against the same kinase panel as that for **19**, revealing that none of five off-target kinases were targeted potently, with percentages of residual kinase activity ranging from 61% to 97% (Fig. 4). The desired selectivity for CDK8 over GSK-3α/β was eventually attained by introduction of a simple amino group to the C2 position of the pyridine core.

2.4. Pharmacokinetic profiling of 42 and 43 in murines

Preclinical pharmacokinetic evaluation is a pivotal component of drug discovery and should be carried out at the very early stage to prioritise the candidates with the best chance of success [66]. Accordingly, two out of the three most potent CDK8 inhibitors (K_i < 0.010 μM), *i.e.*, **42** and **43**, were subjected to *in vivo* single-dose pharmacokinetic studies prior to further *in vitro* biological assessments; the other single-digit nanomolar CDK8 inhibitor, **19**, was not chosen for its poor inhibitory selectivity over GSK-3α/β in the preliminary screening (Fig. 4).

Pharmacokinetic data stated in Table 5 were acquired by treating male Sprague Dawley rats and male BALB/c mice with the same regimens as those for AU1-100 [58]. Briefly, rats were administered **42** or **43** *via* an intravenous (IV) injection at 5 mg/kg or *per os* (PO) at 20 mg/kg, whilst mice were given **42** or **43** IV at 2 mg/kg or PO at 10 mg/kg. After IV administration to rats, concentrations of **42** and **43** in plasma rose up to 9.36 and 11.10 μM within 2 and 9 min, and subsequently declined to half the levels at 1.45 and 4.41 h, respectively, giving rise to their respective area under the plasma concentration versus time curve (AUC) values of 8.92 and 18.36 μM·h. The decline in the plasma concentration of each compound was attributed to its extravascular distribution (**42**: V_{dss} = 1.57 L/kg and **43**: V_{dss} = 1.32 L/kg) and its clearance from plasma (**42**: Cl = 1.43 L/h·kg and **43**: Cl = 0.79 L/h·kg). On the other hand, following oral gavage of rats with **42** and **43** separately, their respective concentrations in plasma reached maxima of 3.20 and 1.35 μM at 4 and 5 h, and then were halved approximately 3 and 5 h later, resulting in AUC values of 25.09 and 19.46 μM·h, respectively. In comparison with AU1-100, **42** showed an increased oral AUC value, achieving a significantly improved oral bioavailability in rats (**42**: F = 70% versus AU1-100: F = 38%). In contrast, **43** is less orally bioavailable (F = 26%). The same held true when the three compounds were assessed in mice; **42** and AU1-100 had an identical F value of 33% that was greater than that of **43** (F = 28%). Only **42** was advanced further by virtue of its superior oral bioavailability in rodents, particularly in rats.

Table 3
Chemical structures and biological activities of **5**, **7**, **8** and **25**–**32**.

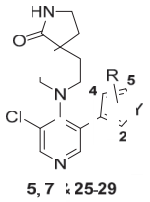

5, 7 & 25-29

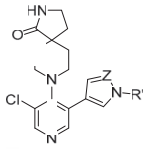

8 & 30-32

Compound	Y/Z	R/R′	CDK8/cyclin C inhibition, K_i (μM)[a]	MV4-11 anti-proliferation, GI_{50} (μM)[b]
5	O	–	0.042	0.75 ± 0.02
25	O	5-CHO	0.185	5.15 ± 0.18
7	S	–	0.018	0.19 ± 0.09
26	S	2-$COCH_3$	4.655	>100
27	S	2-CHO	1.745	28.70 ± 3.54
28	S	4-CHO	0.845	27.10 ± 7.00
29	S	5-CHO	0.052	0.73 ± 0.08
8	C	H	0.014	1.05 ± 0.67
30	N	H	0.254	8.52 ± 0.91
31	N	CH_3	0.230	5.53 ± 1.61
32	N	CHF_2	0.093	6.14 ± 0.86

[a] Inhibition of CDK8/cyclin C was measured with the ^{33}PanQinase® activity assay at ProQinase GmbH, and the K_m value used as the ATP concentration. Each apparent inhibition constant (K_i) was calculated using its corresponding IC_{50} value and the K_m (ATP) value.
[b] GI_{50} values were determined in-house by the 72 h resazurin assay, and are presented as mean ± standard deviation derived from at least two replicates.

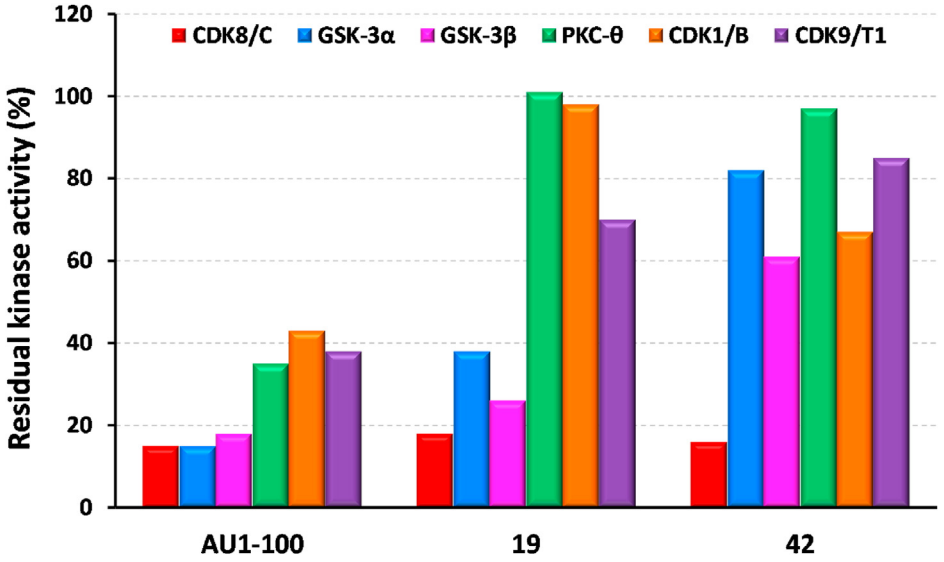

Fig. 4. Kinase inhibition profiles of **19** and **42** (at 1 μM) over a selection of five off-target kinases of AU1-100—GSK-3α/β, PKC-θ, CDK1/cyclin B and CDK9/cyclin T1. Percentages of residual kinase activity of CDK8 and off-target kinases were acquired at ProQinase GmbH and Reaction Biology Corporation, respectively. All the kinase data of AU1-100 were previously reported in Ref. [58], and are included in the figure for the comparison with the corresponding values of **19** and **42**.

Table 4
Chemical structures and biological activities of **42** and **43**.

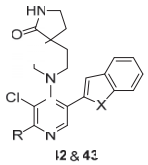

12 & 43

Compound	X	R	CDK8/cyclin C inhibition, K_i (μM)[a]	MV4-11 anti-proliferation, GI_{50} (μM)[b]
AU1-100	O	H	0.014	0.36 ± 0.35
42	O	NH_2	0.009	0.60 ± 0.03
39[c]	S	H	0.014	0.58 ± 0.14
43	S	NH_2	0.007	0.16 ± 0.01
CCT251921	structure in Fig. 1		0.011	0.05 ± 0.01

[a] Inhibition of CDK8/cyclin C was measured with the ^{33}PanQinase® activity assay at ProQinase GmbH, and the K_m value used as the ATP concentration. Each apparent inhibition constant (K_i) was calculated using its corresponding IC_{50} value and the K_m (ATP) value.
[b] GI_{50} values were determined in-house by the 72 h resazurin assay, and are presented as mean ± standard deviation derived from at least two replicates.
[c] Compounds and their biological data were previously reported in Ref. [58].

Table 5
Pharmacokinetic properties of **42** and **43** in rats and mice[a].

Species	Compound	Route	Dose (mg/kg)	V_{dss} (L/kg)	Cl (L/h·kg)	C_{max} (μM)	T_{max} (h)	$T_{1/2}$ (h)	AUC (μM·h)	*F* (%)
Rat	**AU1-100**[b]	IV	5	1.11	1.39	14.40	0.04	0.90	9.70	-
		PO	20	–	–	2.77	2.75	2.24	14.58	***38***
	42	IV	5	1.57	1.43	9.36	0.03	1.45	8.92	-
		PO	20	–	–	3.20	4.00	6.99	25.09	***70***
	43	IV	5	1.32	0.79	11.10	0.15	4.41	18.36	-
		PO	20	–	–	1.35	5.00	10.09	19.46	***26***
Mouse	**AU1-100**[b]	IV	2	1.99	3.78	3.44	0.04	0.34	1.39	-
		PO	10	–	–	5.01	0.42	1.11	2.30	***33***
	42	IV	2	1.24	3.25	4.16	0.05	0.37	1.55	-
		PO	10	–	–	2.23	0.34	3.44	2.56	***33***
	43	IV	2	1.60	2.00	4.96	0.05	0.88	2.40	-
		PO	10	–	–	1.68	0.18	1.67	3.40	***28***

[a] Non-compartmental pharmacokinetic analysis was performed using Phoenix WinNonlin (Certara, St. Louis, MO, USA) for each curve of plasma concentration versus time, and mean values derived from three rats or ten mice are presented.
[b] Pharmacokinetic data of AU1-100 were previously reported in Ref. [58], and are included in the table for the comparison with those of **42** and **43**.

2.5. Physicochemical characterisation of 42

To better understand the pharmacokinetic behaviour of **42** in rodents described above, the compound underwent a physicochemical profiling, with the negative log of the acid dissociation constant (pKa), distribution coefficient (Log D), aqueous solubility, and Caco-2 permeability measured (Table 6). The pKa value of a chemical predicts its ionisation potential that influences the solubility of the chemical through equilibrating the conversion between its neutral and charged forms, and eventually affects its oral absorption [67]. Compound **42** has a pKa value of 5.27 which is greater than that of AU1-100 (pKa = 4.90), suggesting that the former would be more protonated than the latter at, for example, gastric pH of 1.5–3.5 [68]. It is evident that a poor aqueous solubility can limit the absorption of a drug from the gastrointestinal tract, which in turn reduces its oral bioavailability. The

Table 6
Physicochemical properties of **42**.

Physicochemical property[a]		AU1-100[f]	42
Negative log of the acid dissociation constant: pKa[b]		4.90 ± 0.02	5.27 ± 0.01
Aqueous solubility (μM)[c]		10–30	3–20
Distribution coefficient: Log $D_{7.4}$[d]		4.21	4.08
Caco-2 permeability[e]	A—B P_{app} (× 10^{-6} cm/s)	22.9 ± 0.6	29.7 ± 1.9
	B—A P_{app} (× 10^{-6} cm/s)	23.4 ± 3.2	29.8 ± 2.9
	Efflux ratio	1.02	1.00

[a] Physicochemical properties were measured by Cyprotex Discovery Ltd.
[b] Using a fast ultraviolet (UV) spectrometric titration.
[c] By turbidimetry.
[d] Using the shake flask assay with a buffer at pH 7.4.
[e] Using Caco-2 cell line that was derived from a human colon carcinoma and that resembles intestinal epithelial cells. Transport of a compound across the cell monolayer occurs in both directions: apical to basolateral (A—B) and basolateral to apical (B—A). P_{app}: apparent permeability coefficient; efflux ratio = P_{app}(B—A)/P_{app}(A—B).
[f] Physicochemical data of AU1-100 were previously reported in Ref. [58], and are included in the table for the comparison with those of **42**.

turbidimetric solubility of **42** was estimated in between 3 and 20 μM, a span that is similar to that of AU1-100 (10–30 μM). These ranges indicate that both compounds have limited aqueous solubility. Log D of a compound is a measure of its lipophilicity that is a key determinant of the pharmacokinetic behaviour of the compound [67]. The Log $D_{7.4}$ value of **42** was determined to be 4.08, which is below that of AU1-100 (Log $D_{7.4} = 4.21$) and is closer to an optimal range of 0–3 [67]. A compound with its Log D value within this range is typically considered to have a good balance between solubility and permeability as well as to have low metabolic liability. Despite its suboptimal solubility and lipophilicity, **42** possesses high permeability with a passive apparent permeability coefficient (P_{app}(A—B)) value of 29.7×10^{-6} cm/s acquired with the Caco-2 cell-based permeability assay, which compares favourably with that of AU1-100 (P_{app}(A—B) $= 22.9 \times 10^{-6}$ cm/s). Moreover, an efflux ratio of 1.00 for **42** reflects that little or no active efflux occurred in the assay.

2.6. Kinase selectivity profile of 42

Having achieved the selectivity for CDK8 over GSK-3α/β (Fig. 4), **42** was further screened against a panel of 371 kinases at a compound concentration of 1 μM. This concentration is above 110 times greater than CDK8 K_i value of the compound. It was found that only three other kinases, namely leucine-rich repeat kinase 2 (LRRK2), colony stimulating factor 1 receptor (CSF1R, colloquially known as FMS), and FMS-like tyrosine kinase 3 (FLT3), were deprived of more than 50% kinase activity by **42** (Fig. 5). K_i values for the three kinases were later measured to be in a range of 0.051–0.242 μM, which is 5- to 27-time higher than that of CDK8 ($K_i = 0.009$ μM). Further medicinal chemistry optimisation to refine the kinase inhibitory selectivity might not be necessary because all three off-targets are implicated in human cancer. For example, FLT3 is a validated therapeutic target in *FLT3* mutation-positive AML, with two small-molecule inhibitors—midostaurin and gilteritinib—approved for this indication by the United States Food and Drug Administration (US FDA) [69,70], while pathological roles of LRRK2 and FMS in malignancies are emerging [71–75]. To the best of our knowledge, the inhibitory selectivity of **42** for CDK8 is at least comparable to those of known inhibitors of this kinase.

2.7. Safety profile of 42

In addition to a limited degree of CDK8 inhibitory selectivity, AU1-100 exhibited moderate inhibition of two CYP450 enzyme isoforms (*i.e.*, CYP1A: IC_{50} = 7.7 μM and CYP3A4: IC_{50} = 4.6 μM) [58], which might potentially interact with co-administered drugs, leading to adverse drug reactions or toxicity [76]. The specificity for CDK8 was successfully maximised by installation of a primary amino group at the pyridine-C2 position of the compound (Table 4 and Fig. 5). The molecule thus generated, *i.e.*, **42**, was further evaluated *in vitro* for its toxicity potential (Table 7). In contrast to AU1-100, **42** has no inhibitory activity towards CYP1A and CYP3A4 as well as the other three isoforms tested (*i.e.*, CYP2C9, CYP2C19 and CYP2D6), with all IC_{50} values > 25 μM, suggesting a little likelihood of inducing CYP450-mediated drug-drug interactions by **42**. This can be important as combination therapy is prevalent in the current treatments of cancer with kinase inhibitors [70].

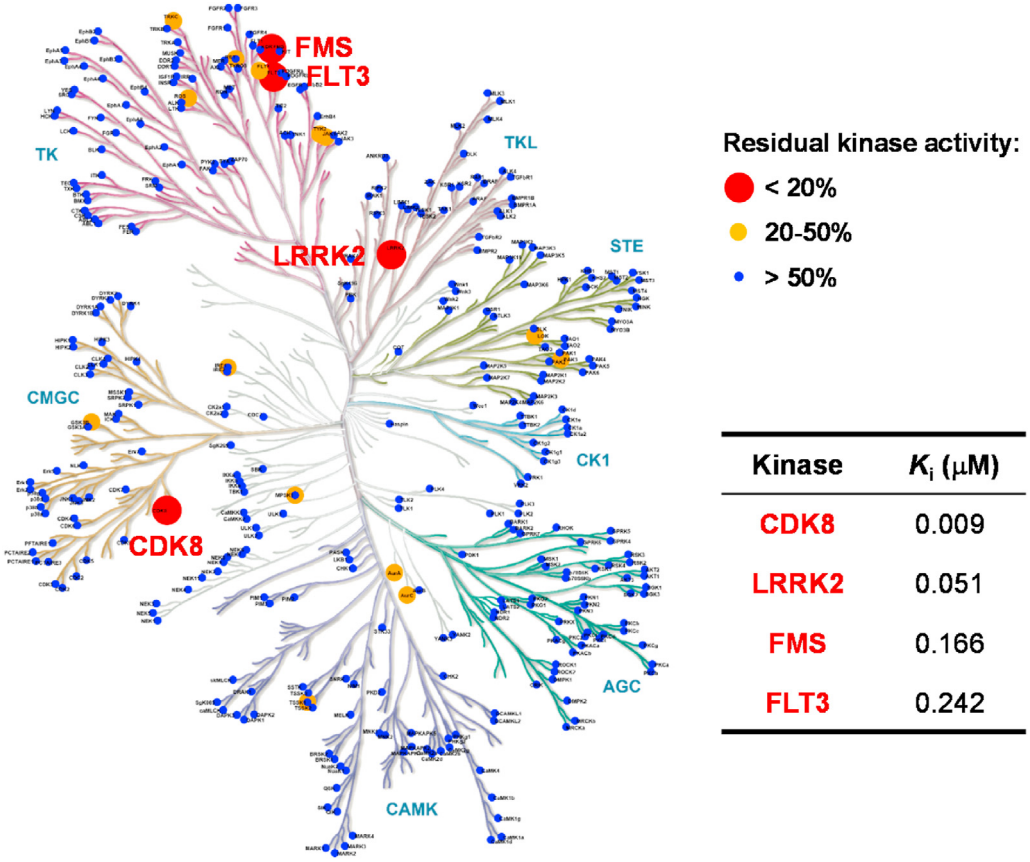

Kinase	K_i (μM)
CDK8	0.009
LRRK2	0.051
FMS	0.166
FLT3	0.242

Fig. 5. Kinase inhibition profile of **42** at 1 μM in a screening against a panel of 371 kinases. The human kinome tree was annotated and generated using $KinMap_{beta}$ (http://www.kinhub.org/kinmap/index.html). Kinase residual activity (%) values were included in Supplementary Data in the form of a spreadsheet file. The K_i value for each kinase with a residual kinase activity of <20% was determined and presented in the table. All the data were acquired at Reaction Biology Corporation and ProQinase GmbH.

Table 7
Pharmaceutical properties of **42**.

Parameter[a]		AU1-100[d]	42
CYP450 inhibition, IC_{50} (μM)[b]	CYP1A	7.7 ± 1.6	>25
	CYP2C9	>25	>25
	CYP2C19	>25	>25
	CYP2D6	>25	>25
	CYP3A4	4.6 ± 0.9	>25
hERG potassium channel inhibition, IC_{50} (μM)[c]		10.9 ± 2.2	>25

[a] Inhibition data were acquired by Cyprotex Discovery Ltd.
[b] Using human liver microsomes in the presence of a CYP450 isoform-specific probe substrate: ethoxyresorufin for CYP1A, tolbutamide for CYP2C9, (*S*)-mephenytoin for CYP2C19, dextromethorphan for CYP2D6, and midazolam for CYP3A4. Typically, potent inhibition: $IC_{50} < 1$ μM; moderate inhibition: $IC_{50} = 1-10$ μM; weak or no inhibition: $IC_{50} > 10$ μM.
[c] Using CHO-hERG cells. Typically, highly potent inhibition: $IC_{50} < 0.1$ μM; potent inhibition: $IC_{50} = 0.1-1$ μM; moderate inhibition: $IC_{50} = 1-10$ μM; weak or no inhibition: $IC_{50} > 10$ μM.
[d] Inhibition data of AU1-100 were previously reported in Ref. [58], and are included in the table for the comparison with those of **42**.

Furthermore, **42** is incapable of inhibiting the human ether-à-go-go related gene (hERG) potassium channel ($IC_{50} > 25$ μM). Blockade of this cardiac ion channel induces QT interval prolongation, which causes potentially fatal ventricular tachyarrhythmia termed *torsade de pointes* [77]. Taken together, **42** has a low risk of causing hepato- and cardio-toxicity.

2.8. Anti-proliferative effects of 42 on cancer cell lines

As described in Section 2.3, discrepancies between CDK8 inhibition and MV4-11 anti-proliferation were noted for a small subset of compounds. This observation called for an interrogation of an appropriate incubation time for the cell viability assay. In that regards, MV4-11 cells were treated with **42** for a period of 24, 48, 72 or 96 h, and GI_{50} values were determined (Fig. S1). The anti-proliferative effect increased up to 72-h treatment, and thereafter started to plateau out. As a result, a 72-h incubation was considered adequate for the cell viability assay and was implemented for screening of **42** against a panel of 12 additional cancer cell lines originated from blood/bone marrow, breast, ovary, pancreas and colon (Fig. 6). Among them, MDA-MB-468 breast cancer cells were most sensitive to **42**, resulting in a $GI_{50} = 0.65$ μM; this degree of growth inhibition was similar to that of MV4-11 cells ($GI_{50} = 0.60$ μM), and is in line with a recent observation that pharmacological inhibition of CDK8 in MDA-MB-468 cells induced apoptosis [78]. The other breast cancer cell lines were 7.5- to 16-fold less sensitive to **42** ($GI_{50} = 4.90-10.37$ μM) than MDA-MB-468, and the rest solid tumour cell lines tested were highly viable ($GI_{50} = 25.80-64.78$ μM), with the exception of A2780 ovarian cancer cells ($GI_{50} = 5.31$ μM). Our previous studies showed that the sensitivity of U-937 and MOLM-13 AML cell lines was only secondary to that of MV4-11 in a screening of AU1-100 against 20 human cell lines (U-937: $GI_{50} = 1.36$ μM and MOLM-13: $GI_{50} = 6.18$ μM versus MV4-11: $GI_{50} = 0.36$ μM) [58]. Similarly, both cell lines remained amenable to **42** at single-digit micromolar concentrations (U-937: $GI_{50} = 4.88$ μM and MOLM-13: $GI_{50} = 5.11$ μM).

2.9. Cellular mechanism of anti-proliferative action of 42

MV4-11 cell line was selected to investigate the mechanism of the anti-proliferative action of **42** by virtue of its highest level of sensitivity towards the compound. Firstly, cellular inhibition of CDK8 kinase activity by **42** was confirmed using western blotting; phosphorylation of STAT1-S727, a documented phosphorylation site for CDK8 [3,79], was dampened, with the total level of STAT1 unaffected, after 24-h incubation with the compound at both 3 and 10 μM (Fig. 7A).

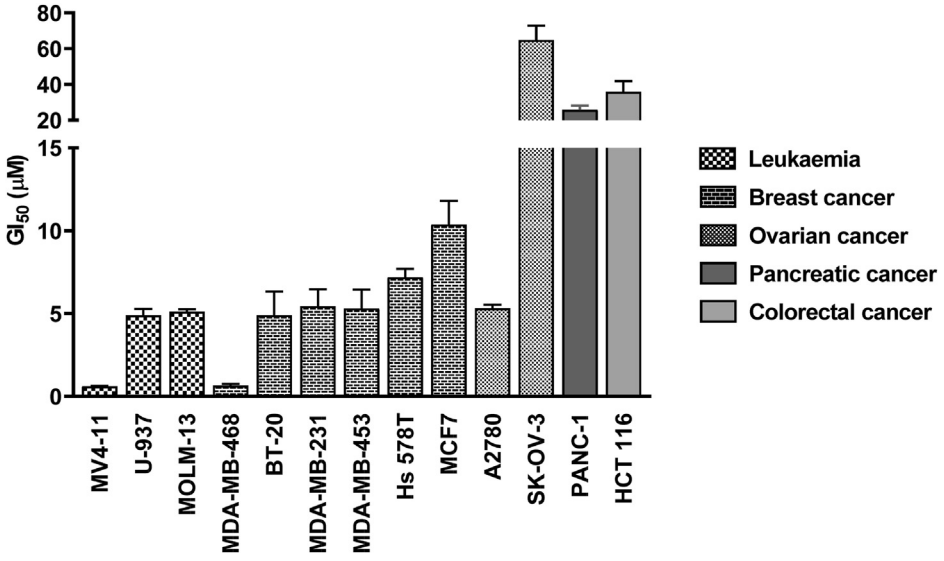

Fig. 6. Anti-proliferative effects of **42** on a panel of 13 human cancer cell lines. GI_{50} values were determined in-house by the 72-h cell viability assay using MTT (adherent cell lines) or resazurin (suspension cell lines).

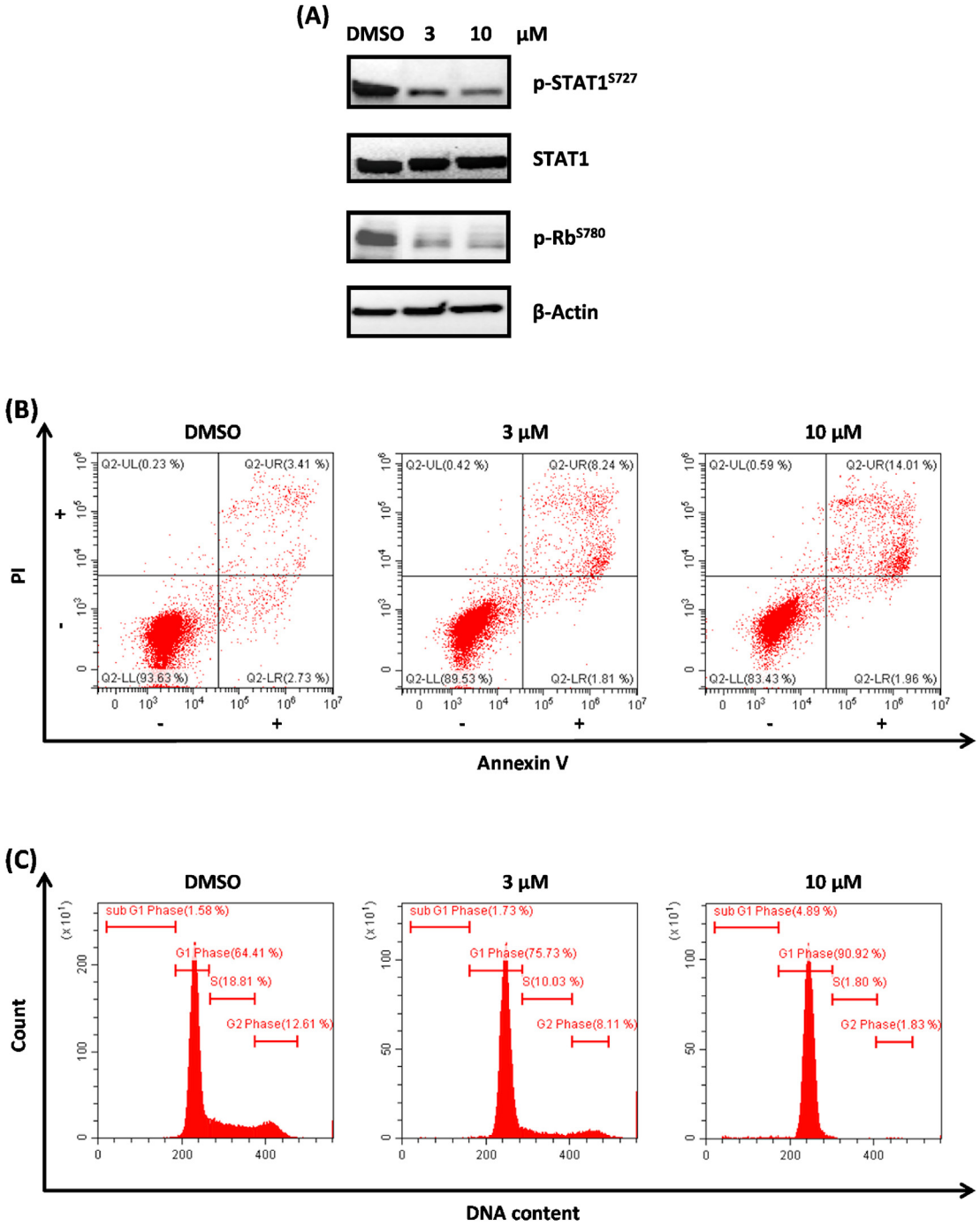

Fig. 7. Cellular mechanism of the anti-proliferative action of **42**. (A) Western blot analysis of MV4-11 cells incubated with **42** for 24 h. β-Actin antibody was used as an internal loading control. (B) Induction of apoptosis by **42** in MV4-11 cells. Cells were exposed to the compound for 72 h and analysed by annexin V/PI staining. The percentage of cells undergoing apoptosis is defined as a sum of early apoptotic (annexin V+/PI-) and late apoptotic (annexin V+/PI+) cell percentages. (C) Cell cycle analysis of MV4-11 cells after incubation with **42** for 72 h. In all experiments, DMSO diluent was employed as a control, and **42** tested at concentrations of 3 and 10 μM.

Programmed cell death takes place mainly through apoptosis [80]. To gauge whether apoptosis contributes to the observed anti-proliferative effect of **42**, MV4-11 cells were double-stained with annexin V and propidium iodide (PI) upon incubation with the compound for 72 h, and the apoptotic subpopulation was detected by flow cytometry (Fig. 7B). In comparison with DMSO diluent, **42** induced approximately 4% and 10% more apoptotic cells (annexin V+/PI- and annexin V+/PI+) at concentrations of 3 and 10 μM, respectively; a finding that correlates with an observation of the downregulated expression of anti-apoptotic protein myeloid cell leukaemia 1 (Mcl-1) in the presence of the compound (Fig. S2).

To further evaluate whether the anti-proliferative effect of **42** results from the blockade of cell cycle progression, MV4-11 cells were incubated with the compound at 3 and 10 μM for 72 h, followed by an flow cytometric analysis of subpopulations at sub-G1, G1, S and G2/M phases of the cell cycle (Fig. 7C). The compound increased the G1-cells at both concentrations (*i.e.*, by 11–27%), in agreement with a reduction in the phosphorylation of

retinoblastoma (Rb) protein at serine 780 (Fig. 7A) because phosphorylated Rb controls the G1-to-S transition of the cell cycle [81].

3. Conclusions

By means of structure-based rational design coupled with modular synthetic approaches developed newly and previously, a number of new tri-/tetra-substituted pyridine derivatives were prepared as CDK8 inhibitors. Compound **42** has been identified as the most promising drug candidate by virtue of its high potency, selectivity and favourable pharmacokinetic properties. **42** inhibited cellular CDK8 evinced by targeting p-STAT1^{S727}, arrested G1 cell cycle and induced apoptosis in MV4-11 cells. Overall, this work has paved the way for further preclinical characterisation of **42** in the context of anti-AML therapy.

4. Experimental

4.1. Method for computational modelling

A crystal structure of CDK8/cyclin C in complex with CCT251545 (PDB ID: 5BNJ) was used for computational modelling. The crystal structure was pre-processed and refined with Schrödinger's Protein Preparation Wizard module (Schrödinger Release 2020-4: Glide, Schrödinger, LLC, New York, NY, 2020) to optimise all atom bonds and orientations. The docking grid was generated to encompass the ATP-binding site. Schrödinger's Extra Precision Glide protocol [59,60,82] was used to dock AU1-100 into the refined protein crystal structure, where the best pose of the compound was generated and compared with that of CCT251545.

4.2. Chemistry

All the reagents (including boronic acids and boronate esters) and non-anhydrous solvents were purchased from Sigma-Aldrich, Merck, Combi-Blocks, AK Scientific, Thermo Fisher Scientific or Ajax Finechem, and were used as received. Anhydrous solvents (*i.e.*, DMF and THF) were collected freshly from a PureSolv™ Micro solvent purification system with activated alumina columns. All the reactions except microwave-assisted syntheses were carried out with continuous magnetic stirring in ordinary glassware. Heating of reactions was conducted with a DrySyn® single- or multi-position heating block (Isleham, UK), and cooling of reactions achieved using an ice-salt or dry ice-acetone bath. Microwave-assisted syntheses were performed in a 10 or 35 mL pressure vessel using a CEM Discover SP and Explorer 48/72/96 microwave system (Matthews, NC, USA) controlled by Synergy software (Firmware version DSCA02.17). ^{1}H and ^{13}C NMR spectra were recorded at 298 K on a Bruker AVANCE III HD 500 spectrometer (Fällanden, Switzerland) (^{1}H at 500.2 MHz and ^{13}C at 125.8 MHz), and were analysed using Bruker Topspin 3.2 software. ^{1}H and ^{13}C NMR spectra are referenced to ^{1}H signals of residual non-deuterated solvents and ^{13}C signals of deuterated solvents, respectively. ^{1}H NMR signals are reported with chemical shift values δ (ppm), multiplicity (s = singlet, d = doublet, t = triplet, q = quartet, dd = doublet of doublets, dt = doublet of triplets, td = triplet of doublets, m = multiplet, br = broad and app = apparent), relative integrals, coupling constants *J* (Hz) and assignments. High resolution mass spectra were recorded on an AB SCIEX TripleTOF 5600 mass spectrometer (Concord, ON, Canada), and the samples subjected to electrospray ionisation (ESI). Melting points were determined using an open capillary on a Stuart SMP10 melting point apparatus or a Mettler Toledo MP50 melting point system, and are uncorrected. The purity of the compounds used for biological evaluation was determined by analytic reversed-phase high-performance liquid chromatography (RP-HPLC), which was carried out on a Shimadzu Prominence UltraFast Liquid Chromatograph (UFLC) system (Kyoto, Japan) equipped with a CBM-20A communications bus module, a DGU-20A5R degassing unit, an LC-20AD liquid chromatograph pump, an SIL-20AHT auto-sampler, an SPD-M20A photo diode array detector, a CTO-20A column oven and a Phenomenex Kinetex C18 column (5 μm, 100 Å, 250 mm × 4.60 mm). Method A (at a flow rate of 1 mL/min, gradient 5%–95% CH_3OH containing 0.1% formic acid (FA) over 7 min followed by 95% CH_3OH containing 0.1% FA over 13 min), method B (at a flow rate of 1 mL/min, gradient 5%–95% CH_3CN containing 0.1% FA over 7 min followed by 95% CH_3CN containing 0.1% FA over 13 min), method C (at a flow rate of 1 mL/min, gradient 5%–95% CH_3OH containing 0.1% FA over 20 min followed by 95% CH_3OH containing 0.1% FA over 5 min) and method D (at a flow rate of 1 mL/min, gradient 5%–95% CH_3CN containing 0.1% FA over 20 min followed by 95% CH_3CN containing 0.1% FA over 5 min) were used for analytic RP-HPLC, and data thus acquired were processed using LabSolutions Analysis Data System. Analytical TLC was performed on Merck silica gel 60 F_{254} pre-coated aluminium plates (0.2 mm) and visualised under UV light (254 nm). Flash column chromatography was carried out using either a conventional glass column loaded with GRACE Davison DAVISIL® silica gel 60 Å (40–63 μm) or a fritted solid loader packed with the same silica gel on a Biotage FlashMaster Personal^{+} flash chromatography system.

General synthetic procedure A: To a suspension of a bromide (1.00 equiv.), a boronic acid or boronate ester (1.05–1.20 equiv.) and $Pd(dppf)Cl_2 \cdot CH_2Cl_2$ (0.05 equiv.) in CH_3CN (150 mM in bromide) was added 0.5 M Na_2CO_3 aqueous solution (1.40 equiv.). The reaction mixture was heated under microwave irradiation at 120–135 °C for 1 h, cooled down, diluted with distilled H_2O, and extracted with DCM (3 ×). The organic extracts were combined, washed with distilled H_2O (1 ×), and concentrated under reduced pressure. The residue was purified by Biotage® FlashMaster Personal^{+} flash chromatography (and, when necessary, triturated or crystallised) to give the desired 5-substituted pyridine.

General synthetic procedure B: To a solution of 4-chloropyridine (1.00 equiv.) in NMP (600 mM in 4-chloropyrdine) were added *tert*-butyl 1-oxo-2,8-diazaspiro[4.5]decane-8-carboxylate (1.00–1.10 equiv.), KF (2.00 equiv.) and triethylamine (3.00 equiv.). The reaction mixture was heated under microwave irradiation at 220–225 °C for 1–2.5 h, cooled down, diluted with distilled H_2O, and extracted with EtOAc (3 ×). The organic extracts were combined, washed with distilled H_2O (3 ×), and concentrated under reduced pressure. The residue was purified by Biotage® FlashMaster Personal^{+} flash chromatography to give the desired spiro compound.

General synthetic procedure C: 4-Methoxybenzyl-protected amine (1.00 equiv.) was dissolved in TFA (50 mM in amine). The reaction mixture was stirred at room temperature overnight and concentrated under reduced pressure. The residue was taken to pH > 11 with saturated aqueous Na_2CO_3 solution and extracted with DCM (3 ×). The organic extracts were combined and concentrated under reduced pressure. The residue was purified by Biotage® FlashMaster Personal^{+} flash chromatography (and crystallised when necessary) to give the desired unprotected form.

3-Bromo-4,5-dichloropyridine (2): To a solution of LDA (2.0 M in THF/heptane/ethylbenzene, 6.25 mL, 12.5 mmol) in anhydrous THF (30 mL) at −78 °C was added a solution of 3-bromo-5-chloropyridine (**1**, 962 mg, 5.00 mmol) in anhydrous THF (10 mL). The reaction mixture was stirred for 1 h, and a solution of hexachloroethane (2.37 g, 10.0 mmol) in anhydrous THF (10 mL) added. The reaction mixture was stirred for 1 h, warmed up to room temperature, quenched with saturated NH_4Cl aqueous solution (30 mL), and extracted with DCM (3 × 100 mL). The organic extracts were combined and concentrated under reduced pressure, and the

residue was purified by Biotage® FlashMaster Personal$^+$ flash chromatography (petroleum benzine ramping to 50% DCM in petroleum benzine) to give **2** as a yellow solid (735 mg, 65%). R_F (DCM:petroleum benzine = 1:4) 0.27. **^{1}H NMR** ($CDCl_3$) δ 8.53 (s, 1H, pyridinyl-H), 8.62 (s, 1H, pyridinyl-H). **^{13}C NMR** ($CDCl_3$) δ 122.1, 131.8, 142.5, 148.5, 150.5.

8-(3-Bromo-5-chloropyridin-4-yl)-2,8-diazaspiro[4.5]decan-1-one (3): To a solution of chloride **2** (1.36 g, 5.99 mmol) and *tert*-butyl 1-oxo-2,8-diazaspiro[4.5]decane-8-carboxylate (1.83 g, 7.20 mmol) in 1-methoxy-2-propanol (10 mL) was added triethylamine (2.51 mL, 18.0 mmol). The reaction mixture was heated under microwave irradiation at 220 °C for 2.5 h, cooled down, diluted with DCM (40 mL), washed with distilled H_2O (2 × 20 mL), and concentrated under reduced pressure. The residue was purified by Biotage® FlashMaster Personal$^+$ flash chromatography (DCM ramping to 4% EtOH in DCM) to give **3** as a beige solid (1.63 g, 79%). R_F (DCM:EtOH = 96:4) 0.31. **^{1}H NMR** ($CDCl_3$) δ 1.54 (d, 2H, *J* 13.0, CH_2), 2.08–2.16 (m, 2H, CH_2), 2.17 (t, 2H, *J* 7.0, CH_2), 3.30–3.44 (m, 4H, 2 × CH_2), 3.39 (t, 2H, *J* 7.0, CH_2), 5.90 (br s, 1H, CONH), 8.35 (s, 1H, pyridinyl-H), 8.49 (s, 1H, pyridinyl-H). **^{13}C NMR** ($CDCl_3$) δ 31.5, 32.6, 39.0, 42.1, 47.0, 119.8, 129.2, 149.8, 151.6, 153.2, 182.1 (two carbon signals overlapping or obscured). **HRMS** (ESI-TOF) 344.0167, 346.0149 & 348.0118 $[M+H]^+$; calcd. for $C_{13}H_{16}BrClN_3O^+$ 344.0160, 346.0140 & 348.0110 $[M+H]^+$.

8-(3-Chloro-5-(furan-2-yl)pyridin-4-yl)-2,8-diazaspiro[4.5]decan-1-one (4): Bromide **3** (173 mg, 502 μmol) and furan-2-ylboronic acid (62 mg, 554 μmol) were reacted at 120 °C using general synthetic procedure A. The residue was purified by Biotage® FlashMaster Personal$^+$ flash chromatography (DCM ramping to 3.5% EtOH in DCM), triturated and washed with *n*-hexane to give **4** as a beige solid (55 mg, 33%). R_F (DCM:EtOH = 96:4) 0.23. **m.p.** 167–168 °C. **^{1}H NMR** (DMSO-d_6) δ 1.33 (app d, 2H, *J* 12.0, CH_2), 1.78 (td, 2H, *J* 11.0 & 2.5, CH_2), 1.94 (t, 2H, *J* 6.0, CH_2), 2.79 (t, 2H, *J* 11.5, CH_2), 3.04 (d, 2H, *J* 11.5, CH_2), 3.17 (t, 2H, *J* 6.0, CH_2), 6.67 (app s, 1H, furanyl-H), 6.77 (app s, 1H, furanyl-H), 7.58 (s, 1H, CONH), 7.87 (app s, 1H, furanyl-H), 8.41 (s, 1H, pyridinyl-H), 8.48 (s, 1H, pyridinyl-H). **^{13}C NMR** (DMSO-d_6) δ 30.5, 31.8, 37.9, 41.3, 45.8, 109.9, 112.2, 123.7, 128.3, 143.9, 148.8, 149.6, 149.9, 152.5, 180.0 (two carbon signals overlapping or obscured). **HRMS** (ESI-TOF) 332.1164 $[M(^{35}Cl)+H]^+$ & 334.1132 $[M(^{37}Cl)+H]^+$; calcd. for $C_{17}H_{19}ClN_3O_2^+$ 332.1160 $[M(^{35}Cl)+H]^+$ & 334.1131 $[M(^{37}Cl)+H]^+$. **Anal. RP-HPLC** Method A: t_R 11.12 min, purity >95%; Method B: t_R 8.83 min, purity >97%.

8-(3-Chloro-5-(furan-3-yl)pyridin-4-yl)-2,8-diazaspiro[4.5]decan-1-one (5): Bromide **3** (173 mg, 502 μmol) and 2-(furan-3-yl)-4,4,5,5-tetramethyl-1,3,2-dioxaborolane (102 mg, 526 μmol) were reacted at 120 °C using general synthetic procedure A. The residue was purified by Biotage® FlashMaster Personal$^+$ flash chromatography (DCM ramping to 4% CH_3OH in DCM), triturated and washed with *n*-hexane to give **5** as a beige solid (90 mg, 54%). R_F (DCM:CH_3OH = 95:5) 0.31. **m.p.** 167–168 °C. **^{1}H NMR** (DMSO-d_6) δ 1.32 (app d, 2H, *J* 12.5, CH_2), 1.76 (td, 2H, *J* 12.0 & 4.0, CH_2), 1.94 (t, 2H, *J* 7.0, CH_2), 2.95 (t, 2H, *J* 11.5, CH_2), 3.04 (dt, 2H, *J* 12.0 & 3.5, CH_2), 3.16 (t, 2H, *J* 7.0, CH_2), 6.72 (app s, 1H, furanyl-H), 7.56 (br s, 1H, CONH), 7.81 (t, 1H, *J* 1.5, furanyl-H), 7.96 (app s, 1H, furanyl-H), 8.29 (s, 1H, pyridinyl-H), 8.42 (s, 1H, pyridinyl-H). **^{13}C NMR** (DMSO-d_6) δ 30.5, 31.8, 37.9, 41.3, 46.7, 112.2, 121.1, 125.9, 127.8, 141.1, 143.7, 149.0, 150.3, 152.5, 180.1 (two carbon signals overlapping or obscured). **HRMS** (ESI-TOF) 332.1164 $[M(^{35}Cl)+H]^+$ & 334.1138 $[M(^{37}Cl)+H]^+$; calcd. for $C_{17}H_{19}ClN_3O_2^+$ 332.1160 $[M(^{35}Cl)+H]^+$ & 334.1131 $[M(^{37}Cl)+H]^+$. **Anal. RP-HPLC** Method A: t_R 10.37 min, purity >95%; Method B: t_R 8.22 min, purity >96%.

8-(3-Chloro-5-(thiophen-2-yl)pyridin-4-yl)-2,8-diazaspiro[4.5]decan-1-one (6): Bromide **3** (173 mg, 502 μmol) and thiophen-2-ylboronic acid (71 mg, 554 μmol) were reacted at 120 °C using general synthetic procedure A. The residue was purified by Biotage® FlashMaster Personal$^+$ flash chromatography (DCM ramping to 2.5% CH_3OH in DCM), triturated and washed with *n*-hexane to give **6** as a pinkish solid (56 mg, 32%). R_F (DCM:CH_3OH = 94:6) 0.36. **m.p.** 175–176 °C. **^{1}H NMR** (DMSO-d_6) δ 1.32 (app d, 2H, *J* 12.5, CH_2), 1.80–1.93 (m, 2H, CH_2), 1.94 (t, 2H, *J* 6.5, CH_2), 3.00 (app s, 4H, CH_2), 3.16 (t, 2H, *J* 6.5, CH_2), 7.18 (t, 1H, *J* 4.0, thiophenyl-H), 7.40 (s, 1H), 7.57 (s, 1H) (total 2H, CONH & thiophenyl-H), 7.71 (d, 1H, *J* 5.0, thiophenyl-H), 8.45 (s, 1H, pyridinyl-H), 8.53 (s, 1H, pyridinyl-H). **^{13}C NMR** (DMSO-d_6) δ 30.4, 31.5, 38.0, 41.4, 46.2, 127.6, 127.9, 128.3, 128.4, 128.9, 136.5, 149.3, 150.0, 152.1, 180.3 (two carbon signals overlapping or obscured). **HRMS** (ESI-TOF) 348.0933 $[M(^{35}Cl)+H]^+$ & 350.0900 $[M(^{37}Cl)+H]^+$; calcd. for $C_{17}H_{19}ClN_3OS^+$ 348.0932 $[M(^{35}Cl)+H]^+$ & 350.0902 $[M(^{37}Cl)+H]^+$. **Anal. RP-HPLC** Method C: t_R 19.30 min, purity >98%; Method D: t_R 12.69 min, purity >98%.

8-(3-Chloro-5-(thiophen-3-yl)pyridin-4-yl)-2,8-diazaspiro[4.5]decan-1-one (7): Bromide **3** (173 mg, 502 μmol) and 4,4,5,5-tetramethyl-2-(thiophen-3-yl)-1,3,2-dioxaborolane (111 mg, 528 μmol) were reacted at 120 °C using general synthetic procedure A. The residue was purified by Biotage® FlashMaster Personal$^+$ flash chromatography (DCM ramping to 4% CH_3OH in DCM), triturated and washed with *n*-hexane to give **7** as a beige solid (82 mg, 47%). R_F (DCM:CH_3OH = 95:5) 0.30. **m.p.** 212–213 °C. **^{1}H NMR** (DMSO-d_6) δ 1.25 (app d, 2H, *J* 13.0, CH_2), 1.72 (td, 2H, *J* 12.5 & 4.0, CH_2), 1.87 (t, 2H, *J* 7.0, CH_2), 2.73 (t, 2H, *J* 11.5, CH_2), 3.01 (app d, 2H, *J* 12.5, CH_2), 3.14 (t, 2H, *J* 7.0, CH_2), 7.19 (dd, 1H, *J* 5.0 & 1.0, thiophenyl-H), 7.54 (s, 1H, CONH), 7.60 (dd, 1H, *J* 2.5 & 1.5, thiophenyl-H), 7.68 (dd, 1H, *J* 5.0 & 3.0, thiophenyl-H), 8.23 (s, 1H, pyridinyl-H), 8.43 (s, 1H, pyridinyl-H). **^{13}C NMR** (DMSO-d_6) δ 30.5, 31.8, 37.9, 41.3, 46.9, 124.3, 126.5, 127.4, 129.1, 129.3, 137.0, 148.9, 150.5, 152.6, 180.0 (two carbon signals overlapping or obscured). **HRMS** (ESI-TOF) 348.0937 $[M(^{35}Cl)+H]^+$ & 350.0909 $[M(^{37}Cl)+H]^+$; calcd. for $C_{17}H_{19}ClN_3OS^+$ 348.0932 $[M(^{35}Cl)+H]^+$ & 350.0902 $[M(^{37}Cl)+H]^+$. **Anal. RP-HPLC** Method A: t_R 10.66 min, purity >98%; Method B: t_R 8.38 min, purity >98%.

8-(3-Chloro-5-(1*H*-pyrrol-3-yl)pyridin-4-yl)-2,8-diazaspiro[4.5]decan-1-one (8): Bromide **3** (173 mg, 502 μmol) and 3-(4,4,5,5-tetramethyl-1,3,2-dioxaborolan-2-yl)-1-(triisopropylsilyl)-1*H*-pyrrole (210 mg, 601 μmol) were reacted at 135 °C using general synthetic procedure A, followed by microwave irradiation at 160 °C for 1 h. The residue was purified by Biotage® FlashMaster Personal$^+$ flash chromatography (DCM ramping to 3.5% CH_3OH in DCM) to give **8** as a yellow solid (38 mg, 23%). R_F (DCM:CH_3OH = 96:4) 0.27. **m.p.** 225–226 °C. **^{1}H NMR** (DMSO-d_6) δ 1.28 (app d, 2H, *J* 13.0, CH_2), 1.77 (td, 2H, *J* 12.0 & 2.5, CH_2), 1.92 (t, 2H, *J* 7.0, CH_2), 2.90 (t, 2H, *J* 11.5, CH_2), 2.96 (d, 2H, *J* 12.0, CH_2), 3.16 (t, 2H, *J* 7.0, CH_2), 6.22 (s, 1H, pyrrolyl-H), 6.85 (s, 1H, pyrrolyl-H), 7.02 (s, 1H, pyrrolyl-H), 7.54 (s, 1H, CONH), 8.26 (s, 1H, pyridinyl-H), 8.30 (s, 1H, pyridinyl-H), 11.05 (s, 1H, pyrrolyl-NH). **^{13}C NMR** (DMSO-d_6) δ 30.4, 31.8, 37.9, 41.4, 46.5, 109.1, 117.4, 118.1, 118.4, 128.2, 130.4, 147.1, 150.5, 152.0, 180.2 (two carbon signals overlapping or obscured). **HRMS** (ESI-TOF) 331.1330 $[M(^{35}Cl)+H]^+$ & 333.1300 $[M(^{37}Cl)+H]^+$; calcd. for $C_{17}H_{20}ClN_4O^+$ 331.1321 $[M(^{35}Cl)+H]^+$ & 333.1291 $[M(^{37}Cl)+H]^+$. **Anal. RP-HPLC** Method C: t_R 12.25 min, purity >98%; Method D: t_R 9.10 min, purity >98%.

8-(3-Chloro-5-(5-methylfuran-2-yl)pyridin-4-yl)-2,8-diazaspiro[4.5]decan-1-one (9): Bromide **3** (173 mg, 502 μmol) and 4,4,5,5-tetramethyl-2-(5-methylfuran-2-yl)-1,3,2-dioxaborolane (125 mg, 601 μmol) were reacted at 135 °C using general synthetic procedure A. The residue was purified by Biotage® FlashMaster Personal$^+$ flash chromatography (DCM ramping to 2.5% CH_3OH in DCM), and crystallised with DCM/*n*-hexane to give **9** as yellow crystals (56 mg, 33%). R_F (DCM:CH_3OH = 94:6) 0.39. **m.p.** 178–179 °C. **^{1}H NMR** (DMSO-d_6) δ 1.34 (app d, 2H, *J* 12.5, CH_2), 1.78 (td, 2H, *J* 11.5 & 1.5, CH_2), 1.95 (t, 2H, *J* 6.5, CH_2), 2.36 (s,

3H, CH_3), 2.80 (t, 2H, *J* 11.5, CH_2), 3.02 (d, 2H, *J* 12.0, CH_2), 3.18 (t, 2H, *J* 6.5, CH_2), 6.26 (s, 1H, furanyl-H), 6.66 (s, 1H, furanyl-H), 7.57 (s, 1H, CONH), 8.39 (s, 1H, pyridinyl-H), 8.44 (s, 1H, pyridinyl-H). **^{13}C NMR** (DMSO-d_6) δ 13.6, 30.6, 31.9, 38.0, 41.3, 45.9, 108.2, 110.5, 124.3, 128.6, 147.3, 149.1, 149.6, 152.2, 152.7, 180.1 (two carbon signals overlapping or obscured). **HRMS** (ESI-TOF) 346.1321 [M(^{35}Cl)+H]$^+$ & 348.1289 [M(^{37}Cl)+H]$^+$; calcd. for $C_{18}H_{21}ClN_3O_2^+$ 346.1317 [M(^{35}Cl)+H]$^+$ & 348.1287 [M(^{37}Cl)+H]$^+$. **Anal. RP-HPLC** Method C: t_R 18.56 min, purity >97%; Method D: t_R 13.09 min, purity >96%.

5-(5-Chloro-4-(1-oxo-2,8-diazaspiro[4.5]decan-8-yl)pyridin-3-yl)furan-2-carbaldehyde (10): Bromide **3** (173 mg, 502 μmol) and (5-formylfuran-2-yl)boronic acid (77 mg, 552 μmol) were reacted at 120 °C using general synthetic procedure A. The residue was purified by Biotage® FlashMaster Personal$^+$ flash chromatography (DCM ramping to 3% CH_3OH in DCM), and crystallised with DCM/*n*-hexane to give **10** as yellow crystals (32 mg, 18%). $\boldsymbol{R_F}$ (DCM:CH_3OH = 94:6) 0.34. **m.p.** 195–196 °C. **^{1}H NMR** (DMSO-d_6) δ 1.33 (app d, 2H, *J* 12.5, CH_2), 1.78 (td, 2H, *J* 12.0 & 2.5, CH_2), 1.90 (t, 2H, *J* 6.0, CH_2), 2.77 (t, 2H, *J* 12.0, CH_2), 3.07 (d, 2H, *J* 12.0, CH_2), 3.16 (t, 2H, *J* 6.0, CH_2), 7.09 (d, 1H, *J* 2.5, furanyl-H), 7.58 (s, 1H, CONH), 7.72 (d, 1H, *J* 2.0, furanyl-H), 8.53 (s, 1H, pyridinyl-H), 8.57 (s, 1H, pyridinyl-H), 9.68 (s, 1H, CHO). **^{13}C NMR** (DMSO-d_6) δ 30.2, 31.7, 37.9, 41.3, 46.2, 112.2, 121.9, 125.1, 128.3, 150.4, 150.7, 152.4, 153.0, 154.6, 178.3, 179.9 (two carbon signals overlapping or obscured). **HRMS** (ESI-TOF) 360.1121 [M(^{35}Cl)+H]$^+$ & 362.1085 [M(^{37}Cl)+H]$^+$; calcd. for $C_{18}H_{19}ClN_3O_3^+$ 360.1109 [M(^{35}Cl)+H]$^+$ & 362.1080 [M(^{37}Cl)+H]$^+$. **Anal. RP-HPLC** Method C: t_R 16.24 min, purity >96%; Method D: t_R 11.64 min, purity >98%.

8-(3-Chloro-5-(5-((ethoxymethoxy)methyl)furan-2-yl)pyridin-4-yl)-2,8-diazaspiro[4.5]decan-1-one (11): Bromide 3 (173 mg, 502 μmol) and 2-(5-((ethoxymethoxy)methyl)furan-2-yl)-4,4,5,5-tetramethyl-1,3,2-dioxaborolane (170 mg, 602 μmol) were reacted at 135 °C using general synthetic procedure A. The residue was purified by Biotage® FlashMaster Personal$^+$ flash chromatography (DCM ramping to 3% CH_3OH in DCM) to give 11 as a beige solid (90 mg, 43%). R_F (DCM:CH_3OH = 94:6) 0.38. m.p. 137–138 °C. ^{1}H NMR (DMSO-d_6) δ 1.13 (t, 3H, *J* 7.0, CH_2CH_3), 1.32 (app d, 2H, *J* 12.5, CH_2), 1.78 (td, 2H, *J* 12.5 & 3.5, CH_2), 1.96 (t, 2H, *J* 6.5, CH_2), 2.78 (t, 2H, *J* 12.0, CH_2), 3.03 (d, 2H, *J* 12.0, CH_2), 3.17 (t, 2H, *J* 6.5, CH_2), 3.54 (q, 2H, *J* 7.0, CH_2CH_3), 4.55 (s, 2H), 4.68 (s, 2H) (total 4H, furanyl-CH_2OCH_2), 6.60 (d, 1H, *J* 2.5, furanyl-H), 6.72 (d, 1H, *J* 2.5, furanyl-H), 7.57 (s, 1H, CONH), 8.39 (s, 1H, pyridinyl-H), 8.47 (s, 1H, pyridinyl-H). ^{13}C NMR (DMSO-d_6) δ 15.1, 30.5, 31.8, 38.0, 41.5, 46.0, 60.6, 62.8, 93.7, 110.1, 111.7, 123.5, 128.4, 149.2, 149.6, 150.0, 152.3, 152.6, 180.1 (two carbon signals overlapping or obscured). HRMS (ESI-TOF) 420.1691 [M(^{35}Cl)+H]$^+$ & 422.1657 [M(^{37}Cl)+H]$^+$; calcd. for $C_{21}H_{27}ClN_3O_4^+$ 420.1685 [M(^{35}Cl)+H]$^+$ & 422.1655 [M(^{37}Cl)+H]$^+$. Anal. RP-HPLC Method C: t_R 18.91 min, purity >95%; Method D: t_R 13.41 min, purity >96%.

8-(3-Chloro-5-(3-methylthiophen-2-yl)pyridin-4-yl)-2,8-diazaspiro[4.5]decan-1-one (12): Bromide **3** (173 mg, 502 μmol) and 4,4,5,5-tetramethyl-2-(3-methylthiophen-2-yl)-1,3,2-dioxaborolane (124 mg, 553 μmol) were reacted at 120 °C using general synthetic procedure A. The residue was purified by Biotage® FlashMaster Personal$^+$ flash chromatography (DCM ramping to 2.5% CH_3OH in DCM), and triturated with *n*-hexane to give **12** as an off-white solid (80 mg, 44%). $\boldsymbol{R_F}$ (DCM:CH_3OH = 94:6) 0.45. **m.p.** 202–203 °C. **^{1}H NMR** (DMSO-d_6) δ 1.26 (app d, 2H, *J* 12.5, CH_2), 1.70 (td, 2H, *J* 12.0 & 4.0, CH_2), 1.83 (t, 2H, *J* 6.5, CH_2), 2.12 (s, 3H, CH_3), 2.67 (t, 2H, *J* 12.0, CH_2), 3.07 (app d, 2H, *J* 12.0, CH_2) 3.12 (t, 2H, *J* 6.5, CH_2), 7.03 (d, 1H, *J* 5.0, thiophenyl-H), 7.53 (s, 1H, CONH), 7.60 (d, 1H, *J* 5.0, thiophenyl-H), 8.17 (s, 1H, pyridinyl-H), 8.47 (s, 1H, pyridinyl-H). **^{13}C NMR** (DMSO-d_6) δ 14.2, 30.5, 31.8, 37.9, 41.3, 46.6, 125.5, 125.9, 127.1, 130.2, 131.7, 135.6, 149.6, 151.7, 154.2, 179.9 (two carbon signals overlapping or obscured). **HRMS** (ESI-TOF) 362.1089 [M(^{35}Cl)+H]$^+$ & 364.1059 [M(^{37}Cl)+H]$^+$; calcd. for $C_{18}H_{21}ClN_3OS^+$ 362.1088 [M(^{35}Cl)+H]$^+$ & 364.1059 [M(^{37}Cl)+H]$^+$. **Anal. RP-HPLC** Method C: t_R 19.56 min, purity >97%; Method D: t_R 12.75 min, purity >97%.

8-(3-Chloro-5-(4-methylthiophen-2-yl)pyridin-4-yl)-2,8-diazaspiro[4.5]decan-1-one (13): Bromide **3** (173 mg, 502 μmol) and 4,4,5,5-tetramethyl-2-(4-methylthiophen-2-yl)-1,3,2-dioxaborolane (124 mg, 553 μmol) were reacted at 120 °C using general synthetic procedure A. The residue was purified by Biotage® FlashMaster Personal$^+$ flash chromatography (DCM ramping to 3% CH_3OH in DCM), triturated and washed with *n*-hexane to give **13** as a beige solid (65 mg, 36%). $\boldsymbol{R_F}$ (DCM:CH_3OH = 94:6) 0.41. **m.p.** 161–162 °C. **^{1}H NMR** (DMSO-d_6) δ 1.33 (app d, 2H, *J* 12.5, CH_2), 1.80–1.93 (m, 2H, CH_2), 1.94 (t, 2H, *J* 6.5, CH_2), 2.26 (s, 3H, CH_3), 2.99 (app s, 4H, 2 × CH_2), 3.16 (t, 2H, *J* 6.5, CH_2), 7.21 (s, 1H, thiophenyl-H), 7.28 (s, 1H, thiophenyl-H), 7.57 (s, 1H, CONH), 8.43 (s, 1H, pyridinyl-H), 8.49 (s, 1H, pyridinyl-H). **^{13}C NMR** (DMSO-d_6) δ 15.5, 30.3, 31.4, 37.9, 41.3, 46.1, 123.5, 128.4, 128.8, 129.9, 136.3, 137.3, 149.1, 149.8, 152.0, 180.1 (two carbon signals overlapping or obscured). **HRMS** (ESI-TOF) 362.1090 [M(^{35}Cl)+H]$^+$ & 364.1060 [M(^{37}Cl)+H]$^+$; calcd. for $C_{18}H_{21}ClN_3OS^+$ 362.1088 [M(^{35}Cl)+H]$^+$ & 364.1059 [M(^{37}Cl)+H]$^+$. **Anal. RP-HPLC** Method A: t_R 12.03 min, purity >95%; Method B: t_R 9.81 min, purity >97%.

8-(3-Chloro-5-(5-methylthiophen-2-yl)pyridin-4-yl)-2,8-diazaspiro[4.5]decan-1-one (14): Bromide **3** (173 mg, 502 μmol) and 4,4,5,5-tetramethyl-2-(5-methylthiophen-2-yl)-1,3,2-dioxaborolane (124 mg, 553 μmol) were reacted at 120 °C using general synthetic procedure A. The residue was purified by Biotage® FlashMaster Personal$^+$ flash chromatography (DCM ramping to 3% CH_3OH in DCM), triturated and washed with *n*-hexane to give **14** as a beige solid (110 mg, 60%). $\boldsymbol{R_F}$ (DCM:CH_3OH = 96:4) 0.26. **m.p.** 172–173 °C. **^{1}H NMR** (DMSO-d_6) δ 1.34 (app d, 2H, *J* 12.5, CH_2), 1.82–1.93 (m, 2H, CH_2), 1.95 (t, 2H, *J* 7.0, CH_2), 2.51 (s, 3H, CH_3), 3.01 (app s, 4H, 2 × CH_2), 3.18 (t, 2H, *J* 7.0, CH_2), 6.87 (d, 1H, *J* 2.0, thiophenyl-H), 7.16 (app s, 1H, thiophenyl-H), 7.59 (s, 1H, CONH), 8.43 (s, 1H, pyridinyl-H), 8.47 (s, 1H, pyridinyl-H). **^{13}C NMR** (DMSO-d_6) δ 15.0, 30.4, 31.4, 37.9, 41.2, 46.1, 125.8, 127.7, 128.4, 128.7, 134.1, 141.5, 148.9, 149.9, 151.8, 180.0 (two carbon signals overlapping or obscured). **HRMS** (ESI-TOF) 362.1090 [M(^{35}Cl)+H]$^+$ & 364.1059 [M(^{37}Cl)+H]$^+$; calcd. for $C_{18}H_{21}ClN_3OS^+$ 362.1088 [M(^{35}Cl)+H]$^+$ & 364.1059 [M(^{37}Cl)+H]$^+$. **Anal. RP-HPLC** Method A: t_R 12.01 min, purity >95%; Method B: t_R 9.73 min, purity >97%.

8-(3-Chloro-5-(5-chlorothiophen-2-yl)pyridin-4-yl)-2,8-diazaspiro[4.5]decan-1-one (15): Bromide **3** (173 mg, 502 μmol) and (5-chlorothiophen-2-yl)boronic acid (90 mg, 554 μmol) were reacted at 120 °C using general synthetic procedure A. The residue was purified by Biotage® FlashMaster Personal$^+$ flash chromatography (DCM ramping to 3% CH_3OH in DCM), and crystallised with DCM/*n*-hexane to give **15** as yellow crystals (21 mg, 11%). $\boldsymbol{R_F}$ (DCM:CH_3OH = 94:6) 0.41. **m.p.** 195–196 °C. **^{1}H NMR** (DMSO-d_6) δ 1.41 (app d, 2H, *J* 13.0, CH_2), 1.92–2.10 (m, 2H, CH_2), 2.02 (t, 2H, *J* 7.0, CH_2), 2.98 (d, 2H, *J* 10.5, CH_2), 3.20 (t, 2H, *J* 6.5, CH_2), 3.23–3.39 (m, 2H, CH_2), 7.19 (d, 1H, *J* 4.0, thiophenyl-H), 7.53 (s, 1H), 7.61 (s, 1H) (total 2H, thiophenyl-H & CONH), 8.46 (s, 1H, pyridinyl-H), 8.79 (s, 1H, pyridinyl-H). **^{13}C NMR** (DMSO-d_6) δ 30.2, 31.0, 32.2, 38.0, 41.1, 45.3, 46.9, 126.8, 127.0, 128.5, 129.7, 130.9, 134.4, 148.4, 149.4, 150.7, 180.1. **HRMS** (ESI-TOF) 382.0544 [M(^{35}Cl/^{35}Cl)+H]$^+$, 384.0514 [M(^{35}Cl/^{37}Cl)+H]$^+$ & 386.0489 [M(^{37}Cl/^{37}Cl)+H]$^+$; calcd. for $C_{17}H_{18}Cl_2N_3OS^+$ 382.0542 [M(^{35}Cl/^{35}Cl)+H]$^+$, 384.0513 [M(^{35}Cl/^{37}Cl)+H]$^+$ & 386.0484 [M(^{37}Cl/^{37}Cl)+H]$^+$. **Anal. RP-HPLC** Method C: t_R 21.27 min, purity >95%; Method D: t_R 15.82 min, purity >96%.

8-(3-(5-Acetylthiophen-2-yl)-5-chloropyridin-4-yl)-2,8-diazaspiro[4.5]decan-1-one (16): Bromide **3** (173 mg, 502 μmol) and (5-acetylthiophen-2-yl)boronic acid (94 mg, 552 μmol) were

reacted at 120 °C using general synthetic procedure A. The residue was purified by Biotage® FlashMaster Personal$^+$ flash chromatography (DCM ramping to 3% CH_3OH in DCM) to give **16** as a tan solid (25 mg, 13%). R_F (DCM:CH_3OH = 94:6) 0.38. **m.p.** 189–190 °C. **^{1}H NMR** (DMSO-d_6) δ 1.35 (app d, 2H, J 13.0, CH_2), 1.85 (td, 2H, J 11.5 & 1.5, CH_2), 1.94 (t, 2H, J 6.5, CH_2), 2.57 (s, 3H, CH_3), 2.97 (t, 2H, J 11.0, CH_2), 3.07 (d, 2H, J 12.0, CH_2), 3.16 (t, 2H, J 6.5, CH_2), 7.45 (app s, 1H, thiophenyl-H), 7.56 (s, 1H, CONH), 7.96 (d, 1H, J 3.5, thiophenyl-H), 8.52 (s, 1H, pyridinyl-H), 8.53 (s, 1H, pyridinyl-H). **^{13}C NMR** (DMSO-d_6) δ 26.7, 30.5, 31.5, 37.9, 41.2, 46.4, 127.0, 128.4, 129.2, 133.9, 144.8, 145.0, 150.1, 150.3, 152.3, 179.9, 191.0 (two carbon signals overlapping or obscured). **HRMS** (ESI-TOF) 390.1034 [M(^{35}Cl)+H]$^+$ & 392.1000 [M(^{37}Cl)+H]$^+$; calcd. for $C_{19}H_{21}ClN_3O_2S^+$ 390.1038 [M(^{35}Cl)+H]$^+$ & 392.1008 [M(^{37}Cl)+H]$^+$. **Anal. RP-HPLC** Method C: t_R 17.97 min, purity >96%; Method D: t_R 13.09 min, purity >96%.

5-(5-Chloro-4-(1-oxo-2,8-diazaspiro[4.5]decan-8-yl)pyridin-3-yl)thiophene-2-carbaldehyde (17): Bromide **3** (173 mg, 502 μmol) and (5-formylthiophen-2-yl)boronic acid (86 mg, 552 μmol) were reacted at 120 °C using general synthetic procedure A. The residue was purified by Biotage® FlashMaster Personal$^+$ flash chromatography (DCM ramping to 3.5% CH_3OH in DCM), and crystallised with DCM/*n*-hexane to give **17** as orange crystals (30 mg, 16%). R_F (DCM:CH_3OH = 94:6) 0.39. **m.p.** 215–216 °C. **^{1}H NMR** (DMSO-d_6) δ 1.35 (app d, 2H, J 12.5, CH_2), 1.85 (td, 2H, J 11.0 & 2.0, CH_2), 1.94 (t, 2H, J 6.5, CH_2), 2.90 (t, 2H, J 10.5, CH_2), 3.07 (app d, 2H, J 11.5, CH_2), 3.16 (t, 2H, J 6.5, CH_2), 7.57 (s, 1H), 7.58 (s, 1H) (total 2H, CONH & thiophenyl-H), 8.07 (d, 1H, J 3.5, thiophenyl-H), 8.53 (s, 1H, pyridinyl-H), 8.58 (s, 1H, pyridinyl-H), 9.96 (s, 1H, CHO). **^{13}C NMR** (DMSO-d_6) δ 30.5, 31.5, 37.9, 41.2, 46.3, 126.8, 128.5, 129.4, 138.0, 144.1, 146.1, 150.0, 150.5, 152.4, 180.0, 184.6 (two carbon signals overlapping or obscured). **HRMS** (ESI-TOF) 376.0885 [M(^{35}Cl)+H]$^+$ & 378.0856 [M(^{37}Cl)+H]$^+$; calcd. for $C_{18}H_{19}ClN_3O_2S^+$ 376.0881 [M(^{35}Cl)+H]$^+$ & 378.0852 [M(^{37}Cl)+H]$^+$. **Anal. RP-HPLC** Method C: t_R 18.06 min, purity >96%; Method D: t_R 12.91 min, purity >95%.

5-(5-Chloro-4-(1-oxo-2,8-diazaspiro[4.5]decan-8-yl)pyridin-3-yl)-3-methylthiophene-2-carbaldehyde (18): Bromide **3** (173 mg, 502 μmol) and (5-formyl-4-methylthiophen-2-yl)boronic acid (94 mg, 552 μmol) were reacted at 120 °C using general synthetic procedure A. The residue was purified by Biotage® FlashMaster Personal$^+$ flash chromatography (DCM ramping to 3% CH_3OH in DCM), and crystallised with DCM/*n*-hexane to give **18** as a yellow solid (30 mg, 15%). R_F (DCM:CH_3OH = 94:6) 0.39. **m.p.** 233–234 °C. **^{1}H NMR** (DMSO-d_6) δ 1.36 (app d, 2H, J 12.5, CH_2), 1.84 (td, 2H, J 11.0 & 1.0, CH_2), 1.95 (t, 2H, J 6.5, CH_2), 2.60 (s, 3H, CH_3), 3.00 (t, 2H, J 10.0, CH_2), 3.07 (d, 2H, J 12.0, CH_2), 3.16 (t, 2H, J 6.5, CH_2), 7.38 (s, 1H), 7.57 (s, 1H) (total 2H, CONH & thiophenyl-H), 8.52 (s, 1H, pyridinyl-H), 8.54 (s, 1H, pyridinyl-H), 10.07 (s, 1H, CHO). **^{13}C NMR** (DMSO-d_6) δ 13.8, 30.5, 31.5, 37.9, 41.1, 46.3, 126.8, 128.4, 132.6, 138.1, 144.9, 147.9, 149.9, 150.4, 152.3, 179.9, 183.7 (two carbon signals overlapping or obscured). **HRMS** (ESI-TOF) 390.1040 [M(^{35}Cl)+H]$^+$ & 392.1006 [M(^{37}Cl)+H]$^+$; calcd. for $C_{19}H_{21}ClN_3O_2S^+$ 390.1038 [M(^{35}Cl)+H]$^+$ & 392.1008 [M(^{37}Cl)+H]$^+$. **Anal. RP-HPLC** Method C: t_R 18.33 min, purity >95%; Method D: t_R 13.61 min, purity >96%.

8-(3-Chloro-5-(5-phenylthiophen-2-yl)pyridin-4-yl)-2,8-diazaspiro[4.5]decan-1-one (19): Bromide **3** (173 mg, 502 μmol) and (5-phenylthiophen-2-yl)boronic acid (113 mg, 554 μmol) were reacted at 120 °C using general synthetic procedure A. The residue was purified by Biotage® FlashMaster Personal$^+$ flash chromatography (DCM ramping to 2.5% CH_3OH in DCM), and crystallised with DCM/*n*-hexane to give **19** as a yellow solid (40 mg, 19%). R_F (DCM:CH_3OH = 94:6) 0.48. **m.p.** 174–175 °C. **^{1}H NMR** (DMSO-d_6) δ 1.37 (app d, 2H, J 12.5, CH_2), 1.98 (t, 2H, J 7.0, CH_2), 2.00–2.10 (m, 2H, CH_2), 3.05 (app d, 2H, J 12.0, CH_2) 3.10–3.25 (m, 2H, CH_2), 3.17 (t, 2H, J 7.0, CH_2), 7.34 (t, 1H, J 7.5, phenyl-H), 7.44 (t, 2H, J 7.5, 2 × phenyl-H), 7.47 (s, 1H), 7.51–7.62 (m, 2H) (total 3H, CONH & 2 × thiophenyl-H), 7.73 (d, 2H, J 7.5, 2 × phenyl-H), 8.45 (s, 1H, pyridinyl-H), 8.65 (s, 1H, pyridinyl-H). **^{13}C NMR** (DMSO-d_6) δ 30.5, 31.4, 38.1, 41.4, 46.2, 123.9, 125.5, 128.1, 128.5, 128.9, 129.4, 133.6, 135.6, 145.2, 149.3, 149.4, 151.7, 180.3 (five carbon signals overlapping or obscured). **HRMS** (ESI-TOF) 424.1239 [M(^{35}Cl)+H]$^+$ & 426.1212 [M(^{37}Cl)+H]$^+$; calcd. for $C_{23}H_{23}ClN_3OS^+$ 424.1245 [M(^{35}Cl)+H]$^+$ & 426.1215 [M(^{37}Cl)+H]$^+$. **Anal. RP-HPLC** Method C: t_R 22.92 min, purity >95%; Method D: t_R 17.65 min, purity >97%.

8-(3-Chloro-5-(5-(pyrrolidin-1-ylmethyl)thiophen-2-yl)pyridin-4-yl)-2,8-diazaspiro[4.5]decan-1-one (20): Bromide **3** (173 mg, 502 μmol) and 1-((5-(4,4,5,5-tetramethyl-1,3,2-dioxaborolan-2-yl)thiophen-2-yl)methyl)pyrrolidine (162 mg, 552 μmol) were reacted at 120 °C using general synthetic procedure A. The residue was purified by Biotage® FlashMaster Personal$^+$ flash chromatography (DCM ramping to 9% CH_3OH in DCM), and crystallised with DCM/*n*-hexane to give **20** as yellow crystals (22 mg, 10%). R_F (DCM:CH_3OH = 9:1) 0.36. **m.p.** 180–181 °C. **^{1}H NMR** (DMSO-d_6) δ 1.32 (app d, 2H, J 13.0, CH_2), 1.71 (app s, 4H, 2 × pyrrolidinyl-CH_2), 1.83 (td, 2H, J 11.5 & 1.5, CH_2), 1.90 (t, 2H, J 6.5, CH_2), 2.52 (app s, 4H, 2 × pyrrolidinyl-CH_2), 2.90 (t, 2H, J 11.0, CH_2), 3.03 (d, 2H, J 12.0, CH_2), 3.16 (t, 2H, J 6.5, CH_2), 3.80 (s, 2H, thiophenyl-CH_2-pyrrolidinyl), 6.97 (s, 1H, thiophenyl-H), 7.13 (s, 1H, thiophenyl-H), 7.55 (s, 1H, CONH), 8.42 (s, 1H, pyridinyl-H), 8.44 (s, 1H, pyridinyl-H). **^{13}C NMR** (DMSO-d_6) δ 23.2, 30.4, 31.5, 37.9, 41.3, 46.3, 53.3, 54.0, 125.4, 127.0, 128.3, 128.5, 135.9, 145.3, 149.1, 150.2, 152.3, 180.0 (four carbon signals overlapping or obscured). **HRMS** (ESI-TOF) 431.1675 [M(^{35}Cl)+H]$^+$ & 433.1636 [M(^{37}Cl)+H]$^+$; calcd. for $C_{22}H_{28}ClN_4OS^+$ 431.1667 [M(^{35}Cl)+H]$^+$ & 433.1637 [M(^{37}Cl)+H]$^+$. **Anal. RP-HPLC** Method C: t_R 14.47 min, purity >95%; Method D: t_R 10.22 min, purity >95%.

8-(3-Chloro-5-(5-(piperidin-1-ylmethyl)thiophen-2-yl)pyridin-4-yl)-2,8-diazaspiro[4.5]decan-1-one (21): Bromide **3** (173 mg, 502 μmol) and 1-((5-(4,4,5,5-tetramethyl-1,3,2-dioxaborolan-2-yl)thiophen-2-yl)methyl)piperidine (170 mg, 553 μmol) were reacted at 120 °C using general synthetic procedure A. The residue was purified by Biotage® FlashMaster Personal$^+$ flash chromatography (DCM ramping to 7% CH_3OH in DCM) to give **21** as a tan solid (125 mg, 56%). R_F (DCM:CH_3OH = 9:1) 0.35. **m.p.** 198–199 °C. **^{1}H NMR** (DMSO-d_6) δ 1.31 (app d, 2H, J 12.0, CH_2), 1.38 (app s, 2H, piperidinyl-CH_2), 1.42–1.60 (m, 4H, 2 × piperidinyl-CH_2), 1.84 (td, 2H, J 12.0 & 2.0, CH_2), 1.90 (t, 2H, J 6.5, CH_2), 2.41 (app s, 4H, 2 × piperidinyl-CH_2), 2.88 (t, 2H, J 11.0, CH_2), 3.04 (d, 2H, J 11.5, CH_2), 3.15 (t, 2H, J 6.5, CH_2), 3.67 (s, 2H, thiophenyl-CH_2-piperidinyl), 6.96 (d, 1H, J 3.0, thiophenyl-H), 7.14 (d, 1H, J 2.5, thiophenyl-H), 7.55 (s, 1H, CONH), 8.41 (s, 1H, pyridinyl-H), 8.44 (s, 1H, pyridinyl-H). **^{13}C NMR** (DMSO-d_6) δ 24.0, 25.5, 30.4, 31.5, 37.8, 41.2, 46.3, 53.7, 57.3, 126.0, 127.1, 128.2, 128.4, 136.2, 144.5, 149.1, 150.2, 152.3, 179.9 (four carbon signals overlapping or obscured). **HRMS** (ESI-TOF) 445.1827 [M(^{35}Cl)+H]$^+$ & 447.1781 [M(^{37}Cl)+H]$^+$; calcd. for $C_{23}H_{30}ClN_4OS^+$ 445.1823 [M(^{35}Cl)+H]$^+$ & 447.1794 [M(^{37}Cl)+H]$^+$. **Anal. RP-HPLC** Method C: t_R 14.64 min, purity >97%; Method D: t_R 10.64 min, purity >97%.

8-(3-Chloro-5-(5-(morpholinomethyl)thiophen-2-yl)pyridin-4-yl)-2,8-diazaspiro[4.5]decan-1-one (22): Bromide **3** (173 mg, 502 μmol) and 4-((5-(4,4,5,5-tetramethyl-1,3,2-dioxaborolan-2-yl)thiophen-2-yl)methyl)morpholine (171 mg, 553 μmol) were reacted at 120 °C using general synthetic procedure A. The residue was purified by Biotage® FlashMaster Personal$^+$ flash chromatography (DCM ramping to 5% CH_3OH in DCM) to give **22** as a tan solid (100 mg, 45%). R_F (DCM:CH_3OH = 94:6) 0.40. **m.p.** 231–232 °C. **^{1}H NMR** (DMSO-d_6) δ 1.31 (app d, 2H, J 12.5, CH_2), 1.84 (td, 2H, J 11.5 & 1.5, CH_2), 1.90 (t, 2H, J 6.5, CH_2), 2.44 (app s, 4H,

2 × morpholinyl-CH_2), 2.91 (t, 2H, *J* 11.5, CH_2), 3.03 (d, 2H, *J* 12.0, CH_2), 3.16 (t, 2H, *J* 6.5, CH_2), 3.60 (app s, 4H, 2 × morpholinyl-CH_2), 3.71 (s, 2H, thiophenyl-CH_2-morpholinyl), 7.00 (d, 1H, *J* 2.5, thiophenyl-H), 7.17 (app s, 1H, thiophenyl-H), 7.55 (s, 1H, CONH), 8.43 (s, 1H, pyridinyl-H), 8.44 (s, 1H, pyridinyl-H). **^{13}C NMR** (DMSO-d_6) δ 30.4, 31.5, 37.9, 41.3, 46.3, 53.0, 56.9, 66.2, 126.5, 127.1, 128.3, 128.6, 136.5, 143.6, 149.2, 150.1, 152.2, 180.0 (four carbon signals overlapping or obscured). **HRMS** (ESI-TOF) 447.1599 [M(^{35}Cl)+H]$^+$ & 449.1568 [M(^{37}Cl)+H]$^+$; calcd. for $C_{22}H_{28}ClN_4O_2S^+$ 447.1616 [M(^{35}Cl)+H]$^+$ & 449.1587 [M(^{37}Cl)+H]$^+$. **Anal. RP-HPLC** Method C: t_R 14.03 min, purity >98%; Method D: t_R 10.07 min, purity >97%.

***Tert*-butyl 4-((5-(5-chloro-4-(1-oxo-2,8-diazaspiro[4.5]decan-8-yl)pyridin-3-yl)thiophen-2-yl)methyl)piperazine-1-carboxylate (23)**: Bromide **3** (173 mg, 502 μmol) and *tert*-butyl 4-((5-(4,4,5,5-tetramethyl-1,3,2-dioxaborolan-2-yl)thiophen-2-yl) methyl)piperazine-1-carboxylate (246 mg, 602 μmol) were reacted at 135 °C using general synthetic procedure A. The residue was purified by Biotage® FlashMaster Personal$^+$ flash chromatography (DCM ramping to 4% CH_3OH in DCM), and crystallised with DCM/*n*-hexane to give **23** as a yellowish solid (112 mg, 41%). R_F (DCM:CH_3OH = 96:4) 0.32. **m.p.** 184–185 °C. **^{1}H NMR** (DMSO-d_6) δ 1.32 (app d, 2H, *J* 12.5, CH_2), 1.38 (s, 9H, C(CH_3)$_3$), 1.86 (td, 2H, *J* 11.5 & 1.5, CH_2), 1.91 (t, 2H, *J* 6.5, CH_2), 2.41 (app s, 4H, 2 × piperazinyl-CH_2), 2.92 (t, 2H, *J* 11.0, CH_2), 3.02 (d, 2H, *J* 12.0, CH_2), 3.16 (t, 2H, *J* 6.5, CH_2), 3.74 (s, 2H, thiophenyl-CH_2-piperazinyl), 6.99 (d, 1H, *J* 3.0, thiophenyl-H), 7.18 (app s, 1H, thiophenyl-H), 7.56 (s, 1H, CONH), 8.44 (s, 2H, 2 × pyridinyl-H) (four proton signals overlapping or obscured). **^{13}C NMR** (DMSO-d_6) δ 28.1, 30.3, 31.5, 37.9, 41.2, 46.3, 52.2, 56.4, 78.8, 126.4, 127.1, 128.3, 128.6, 136.3, 143.6, 149.1, 150.0, 152.1, 153.9, 180.0 (seven carbon signals overlapping or obscured). **HRMS** (ESI-TOF) 546.2301 [M(^{35}Cl)+H]$^+$ & 548.2252 [M(^{37}Cl)+H]$^+$; calcd. for $C_{27}H_{37}ClN_5O_3S^+$ 546.2300 [M(^{35}Cl)+H]$^+$ & 548.2271 [M(^{37}Cl)+H]$^+$. **Anal. RP-HPLC** Method C: t_R 17.50 min, purity >99%; Method D: t_R 12.45 min, purity >99%.

8-(3-Chloro-5-(1-methyl-1*H*-pyrrol-2-yl)pyridin-4-yl)-2,8-diazaspiro[4.5]decan-1-one (24): Bromide **3** (173 mg, 502 μmol) and 1-methyl-2-(4,4,5,5-tetramethyl-1,3,2-dioxaborolan-2-yl)-1*H*-pyrrole (125 mg, 604 μmol) were reacted at 135 °C using general synthetic procedure A. The residue was purified by Biotage® FlashMaster Personal$^+$ flash chromatography (DCM ramping to 2.5% CH_3OH in DCM) to give **24** as a yellow solid (80 mg, 46%). R_F (DCM:CH_3OH = 96:4) 0.31. **m.p.** 188–189 °C. **^{1}H NMR** (DMSO-d_6) δ 1.24 (app d, 2H, *J* 12.5, CH_2), 1.68 (td, 2H, *J* 12.0 & 4.0, CH_2), 1.83 (t, 2H, *J* 6.5, CH_2), 2.59 (t, 2H, *J* 12.0, CH_2), 3.04 (d, 2H, *J* 12.5, CH_2), 3.12 (t, 2H, *J* 6.5, CH_2), 3.46 (s, 3H, CH_3), 6.01 (app s, 1H, pyrrolyl-H), 6.12 (app s, 1H, pyrrolyl-H), 6.88 (app s, 1H, pyrrolyl-H), 7.53 (s, 1H, CONH), 8.17 (s, 1H, pyridinyl-H), 8.44 (s, 1H, pyridinyl-H). **^{13}C NMR** (DMSO-d_6) δ 30.6, 31.9, 34.1, 37.8, 41.3, 46.5, 107.6, 110.7, 123.2, 124.6, 126.8, 127.1, 149.3, 151.8, 154.2, 179.9 (two carbon signals overlapping or obscured). **HRMS** (ESI-TOF) 345.1475 [M(^{35}Cl)+H]$^+$ & 347.1441 [M(^{37}Cl)+H]$^+$; calcd. for $C_{18}H_{22}ClN_4O^+$ 345.1477 [M(^{35}Cl)+H]$^+$ & 347.1447 [M(^{37}Cl)+H]$^+$. **Anal. RP-HPLC** Method C: t_R 13.84 min, purity >98%; Method D: t_R 10.45 min, purity >96%.

4-(5-Chloro-4-(1-oxo-2,8-diazaspiro[4.5]decan-8-yl)pyridin-3-yl)furan-2-carbaldehyde (25): Bromide **3** (173 mg, 502 μmol) and 4-(4,4,5,5-tetramethyl-1,3,2-dioxaborolan-2-yl)furan-2-carbaldehyde (123 mg, 554 μmol) were reacted at 120 °C using general synthetic procedure A. The residue was purified by Biotage® FlashMaster Personal$^+$ flash chromatography (DCM ramping to 4% EtOH in DCM) to give **25** as a yellow solid (38 mg, 21%). R_F (DCM:CH_3OH = 94:6) 0.40. **m.p.** 184–185 °C. **^{1}H NMR** (DMSO-d_6) δ 1.33 (app d, 2H, *J* 12.5, CH_2), 1.75 (td, 2H, *J* 11.5 & 1.5, CH_2), 1.95 (t, 2H, *J* 6.5, CH_2), 2.95 (t, 2H, *J* 11.5, CH_2), 3.08 (d, 2H, *J* 12.5, CH_2), 3.16 (t, 2H, *J* 6.5, CH_2), 7.57 (s, 1H, CONH), 7.76 (s, 1H, furanyl-H), 8.34 (s, 1H), 8.36 (s, 1H) (total 2H, furanyl-H & pyridinyl-H), 8.48 (s, 1H, pyridinyl-H), 9.68 (s, 1H, CHO). **^{13}C NMR** (DMSO-d_6) δ 30.6, 31.8, 37.9, 41.3, 46.9, 123.6, 123.9, 124.1, 127.7, 147.0, 149.8, 150.4, 152.5, 152.6, 178.8, 180.0 (two carbon signals overlapping or obscured). **HRMS** (ESI-TOF) 360.1098 [M(^{35}Cl)+H]$^+$ & 362.1062 [M(^{37}Cl)+H]$^+$; calcd. for $C_{18}H_{19}ClN_3O_3^+$ 360.1109 [M(^{35}Cl)+H]$^+$ & 362.1080 [M(^{37}Cl)+H]$^+$. **Anal. RP-HPLC** Method C: t_R 14.19 min, purity >95%; Method D: t_R 10.20 min, purity >97%.

8-(3-(2-Acetylthiophen-3-yl)-5-chloropyridin-4-yl)-2,8-diazaspiro[4.5]decan-1-one (26): Bromide **3** (173 mg, 502 μmol) and (2-acetylthiophen-3-yl)boronic acid (102 mg, 600 μmol) were reacted at 135 °C using general synthetic procedure A. The residue was purified by Biotage® FlashMaster Personal$^+$ flash chromatography (DCM ramping to 3.5% EtOH in DCM) to give **26** as a straw solid (130 mg, 66%). R_F (DCM:EtOH = 94:6) 0.42. **m.p.** 209–210 °C. **^{1}H NMR** (DMSO-d_6) δ 1.10–1.30 (m, 2H, CH_2), 1.45–1.70 (m, 2H, CH_2), 1.70–1.90 (m, 2H, CH_2), 2.31 (s, 3H, CH_3), 2.50–2.60 (m, 2H, CH_2), 2.60–2.75 (m, 1H, C*H*H), 2.85–3.05 (m, 1H, CH*H*), 3.10 (t, 2H, *J* 6.5, CH_2), 7.16 (d, 1H, *J* 5.0, thiophenyl-H), 7.51 (s, 1H, CONH), 8.02 (d, 1H, *J* 5.0, thiophenyl-H), 8.14 (s, 1H, pyridinyl-H), 8.46 (s, 1H, pyridinyl-H). **^{13}C NMR** (DMSO-d_6) δ 29.3, 30.6, 31.8, 31.9, 37.9, 41.2, 46.7, 47.2, 126.6, 128.6, 132.2, 133.1, 138.7, 141.0, 149.6, 150.0, 153.0, 179.9, 190.2. **HRMS** (ESI-TOF) 390.1047 [M(^{35}Cl)+H]$^+$ & 392.1014 [M(^{37}Cl)+H]$^+$; calcd. for $C_{19}H_{21}ClN_3O_2S^+$ 390.1038 [M(^{35}Cl)+H]$^+$ & 392.1008 [M(^{37}Cl)+H]$^+$. **Anal. RP-HPLC** Method C: t_R 13.78 min, purity >98%; Method D: t_R 10.21 min, purity >98%.

3-(5-Chloro-4-(1-oxo-2,8-diazaspiro[4.5]decan-8-yl)pyridin-3-yl)thiophene-2-carbaldehyde (27): Bromide **3** (173 mg, 502 μmol) and (2-formylthiophen-3-yl)boronic acid (86 mg, 553 μmol) were reacted at 120 °C using general synthetic procedure A. The residue was purified by Biotage® FlashMaster Personal$^+$ flash chromatography (DCM ramping to 3% CH_3OH in DCM), and crystallised with DCM/*n*-hexane to give **27** as a yellow solid (60 mg, 32%). R_F (DCM:CH_3OH = 94:6) 0.41. **m.p.** 229–230 °C. **^{1}H NMR** (DMSO-d_6) δ 1.23 (app d, 2H, *J* 12.5, CH_2), 1.64 (app s, 2H, CH_2), 1.82 (t, 2H, *J* 6.0, CH_2), 2.55–2.80 (m, 2H, CH_2), 2.95–3.25 (m, 2H, CH_2), 3.11 (t, 2H, *J* 6.5, CH_2), 7.28 (d, 1H, *J* 4.5, thiophenyl-H), 7.52 (s, 1H, CONH), 8.21 (d, 1H, *J* 4.5, thiophenyl-H), 8.28 (s, 1H, pyridinyl-H), 8.52 (s, 1H, pyridinyl-H), 9.67 (s, 1H, CHO). **^{13}C NMR** (DMSO-d_6) δ 30.6, 31.9, 37.9, 41.2, 47.1, 125.9, 127.0, 132.4, 135.4, 139.0, 145.6, 150.4, 150.9, 153.5, 180.0, 184.0 (two carbon signals overlapping or obscured). **HRMS** (ESI-TOF) 376.0879 [M(^{35}Cl)+H]$^+$ & 378.0848 [M(^{37}Cl)+H]$^+$; calcd. for $C_{18}H_{19}ClN_3O_2S^+$ 376.0881 [M(^{35}Cl)+H]$^+$ & 378.0852 [M(^{37}Cl)+H]$^+$. **Anal. RP-HPLC** Method C: t_R 15.93 min, purity >97%; Method D: t_R 11.05 min, purity >98%.

4-(5-Chloro-4-(1-oxo-2,8-diazaspiro[4.5]decan-8-yl)pyridin-3-yl)thiophene-3-carbaldehyde (28): Bromide **3** (173 mg, 502 μmol) and (4-formylthiophen-3-yl)boronic acid (94 mg, 602 μmol) were reacted at 135 °C using general synthetic procedure A. The residue was purified by Biotage® FlashMaster Personal$^+$ flash chromatography (DCM ramping to 4% EtOH in DCM) to give **28** as a beige solid (70 mg, 37%). R_F (DCM:EtOH = 94:6) 0.40. **m.p.** 208–209 °C. **^{1}H NMR** (DMSO-d_6) δ 1.18 (app d, 2H, *J* 12.5, CH_2), 1.55 (app t, 2H, *J* 10.0, CH_2), 1.79 (t, 2H, *J* 6.5, CH_2), 2.61 (t, 2H, *J* 10.5, CH_2), 3.00 (d, 2H, *J* 10.0, CH_2), 3.10 (t, 2H, *J* 6.5, CH_2), 7.51 (s, 1H, CONH), 7.65 (d, 1H, *J* 2.5, thiophenyl-H), 8.12 (s, 1H, pyridinyl-H), 8.46 (s, 1H, pyridinyl-H), 8.70 (d, 1H, *J* 2.0, thiophenyl-H), 9.79 (s, 1H, CHO). **^{13}C NMR** (DMSO-d_6) δ 30.5, 31.8, 37.8, 41.1, 46.9, 126.7, 127.8, 128.4, 135.7, 139.9, 140.1, 149.6, 150.4, 153.4, 179.9, 185.8 (two carbon signals overlapping or obscured). **HRMS** (ESI-TOF) 376.0875 [M(^{35}Cl)+H]$^+$ & 378.0837 [M(^{37}Cl)+H]$^+$; calcd. for $C_{18}H_{19}ClN_3O_2S^+$ 376.0881 [M(^{35}Cl)+H]$^+$ & 378.0852 [M(^{37}Cl)+H]$^+$. **Anal. RP-HPLC** Method C: t_R 12.74 min, purity >97%; Method D: t_R 9.52 min, purity >98%.

4-(5-Chloro-4-(1-oxo-2,8-diazaspiro[4.5]decan-8-yl)pyridin-

3-yl)thiophene-2-carbaldehyde (29): Bromide **3** (173 mg, 502 μmol) and (5-formylthiophen-3-yl)boronic acid (86 mg, 553 μmol) were reacted at 120 °C using general synthetic procedure A. The residue was purified by Biotage® FlashMaster Personal$^+$ flash chromatography (DCM ramping to 3% CH_3OH in DCM), and crystallised with DCM/*n*-hexane to give **29** as a yellowish solid (110 mg, 58%). R_F (DCM:CH_3OH = 94:6) 0.29. **m.p.** 203−204 °C. **^{1}H NMR** (DMSO-d_6) δ 1.27 (app d, 2H, *J* 12.5, CH_2), 1.70 (dt, 2H, *J* 11.5 & 1.5, CH_2), 1.89 (t, 2H, *J* 6.5, CH_2), 2.80 (t, 2H, *J* 11.5, CH_2), 3.06 (app d, 2H, *J* 12.5, CH_2), 3.14 (t, 2H, *J* 6.5, CH_2), 7.54 (s, 1H, CONH), 8.12 (s, 1H, thiophenyl-H), 8.18 (s, 1H, thiophenyl-H), 8.30 (s, 1H, pyridinyl-H), 8.48 (s, 1H, pyridinyl-H), 10.00 (s, 1H, CHO). **^{13}C NMR** (DMSO-d_6) δ 30.6, 31.8, 37.9, 41.3, 47.1, 127.4, 127.9, 134.0, 138.4, 139.2, 143.5, 149.6, 150.3, 152.7, 180.0, 184.6 (two carbon signals overlapping or obscured). **HRMS** (ESI-TOF) 376.0877 [M(^{35}Cl)+H]$^+$ & 378.0848 [M(^{37}Cl)+H]$^+$; calcd. for $C_{18}H_{19}ClN_3O_2S^+$ 376.0881 [M(^{35}Cl)+H]$^+$ & 378.0852 [M(^{37}Cl)+H]$^+$. **Anal. RP-HPLC** Method C: t_R 16.40 min, purity >96%; Method D: t_R 10.80 min, purity >97%.

8-(3-Chloro-5-(1*H*-pyrazol-4-yl)pyridin-4-yl)-2,8-diazaspiro [4.5]decan-1-one (30): Bromide **3** (345 mg, 1.00 mmol) and *tert*-butyl 4-(4,4,5,5-tetramethyl-1,3,2-dioxaborolan-2-yl)-1*H*-pyrazole-1-carboxylate (324 mg, 1.10 mmol) were reacted at 120 °C using general synthetic procedure A. The residue was purified by Biotage® FlashMaster Personal$^+$ flash chromatography (DCM ramping to 7% CH_3OH in DCM), and crystallised with DCM to give **30** as white crystals (145 mg, 44%). R_F (DCM:CH_3OH = 94:6) 0.15. **m.p.** 233−234 °C. **^{1}H NMR** (DMSO-d_6) δ 1.30 (app d, 2H, *J* 13.0, CH_2), 1.76 (td, 2H, *J* 10.5 & 5.0, CH_2), 1.94 (t, 2H, *J* 6.5, CH_2), 2.84−3.02 (m, 4H, 2 × CH_2), 3.16 (t, 2H, *J* 6.5, CH_2), 7.56 (s, 1H), 7.87 (app s, 2H), 8.32 (s, 1H), 8.36 (s, 1H) (total 5H, CONH & 2 × pyrazolyl-H & 2 × pyridinyl-H), 13.09 (br s, 1H, pyrazolyl-NH). **^{13}C NMR** (DMSO-d_6) δ 30.5, 31.8, 37.9, 41.3, 46.6, 115.7, 127.0, 128.3, 148.2, 150.4, 152.1, 180.1 (four carbon signals overlapping or obscured). **HRMS** (ESI-TOF) 332.1272 [M(^{35}Cl)+H]$^+$ & 334.1242 [M(^{37}Cl)+H]$^+$; calcd. for $C_{16}H_{19}ClN_5O^+$ 332.1273 [M(^{35}Cl)+H]$^+$ & 334.1243 [M(^{37}Cl)+H]$^+$. **Anal. RP-HPLC** Method C: t_R 13.74 min, purity >99%; Method D: t_R 8.54 min, purity >99%.

8-(3-Chloro-5-(1-methyl-1*H*-pyrazol-4-yl)pyridin-4-yl)-2,8-diazaspiro[4.5]decan-1-one (31): Bromide **3** (190 mg, 551 μmol) and 1-methyl-4-(4,4,5,5-tetramethyl-1,3,2-dioxaborolan-2-yl)-1*H*-pyrazole (121 mg, 582 μmol) were reacted at 120 °C using general synthetic procedure A. The residue was purified by Biotage® FlashMaster Personal$^+$ flash chromatography (DCM ramping to 7% EtOH in DCM), and triturated with *n*-hexane to give **31** as a beige solid (80 mg, 42%). R_F (DCM:EtOH = 93:7) 0.22. **m.p.** 182−183 °C. **^{1}H NMR** (DMSO-d_6) δ 1.31 (app d, 2H, *J* 13.0, CH_2), 1.76 (td, 2H, *J* 11.5 & 4.0, CH_2), 1.95 (t, 2H, *J* 7.0, CH_2), 2.85−3.00 (m, 4H, 2 × CH_2), 3.17 (t, 2H, *J* 7.0, CH_2), 3.89 (s, 3H, CH_3), 7.56 (s, 1H, CONH), 7.64 (s, 1H, pyrazolyl-H), 7.96 (s, 1H, pyrazolyl-H), 8.27 (s, 1H, pyridinyl-H), 8.35 (s, 1H, pyridinyl-H). **^{13}C NMR** (DMSO-d_6) δ 30.6, 31.8, 38.1, 38.8, 41.4, 46.8, 116.5, 126.7, 128.3, 130.3, 138.7, 148.3, 150.3, 152.1, 180.3 (two carbon signals overlapping or obscured). **HRMS** (ESI-TOF) 346.1430 [M(^{35}Cl)+H]$^+$ & 348.1398 [M(^{37}Cl)+H]$^+$; calcd. for $C_{17}H_{21}ClN_5O^+$ 346.1429 [M(^{35}Cl)+H]$^+$ & 348.1400 [M(^{37}Cl)+H]$^+$. **Anal. RP-HPLC** Method A: t_R 9.73 min, purity >99%; Method B: t_R 7.62 min, purity >99%.

8-(3-Chloro-5-(1-(difluoromethyl)-1*H*-pyrazol-4-yl)pyridin-4-yl)-2,8-diazaspiro[4.5]decan-1-one (32): Bromide **3** (173 mg, 502 μmol) and 1-(difluoromethyl)-4-(4,4,5,5-tetramethyl-1,3,2-dioxaborolan-2-yl)-1*H*-pyrazole (148 mg, 606 μmol) were reacted at 135 °C using general synthetic procedure A. The residue was purified by Biotage® FlashMaster Personal$^+$ flash chromatography (DCM ramping to 3.5% CH_3OH in DCM) to give **32** as a pinkish solid (128 mg, 67%). R_F (DCM:CH_3OH = 94:6) 0.26. **m.p.** 196−197 °C. **^{1}H NMR** (DMSO-d_6) δ 1.31 (app d, 2H, *J* 12.5, CH_2), 1.74 (td, 2H, *J* 11.5 & 2.5, CH_2), 1.93 (t, 2H, *J* 6.5, CH_2), 2.90 (t, 2H, *J* 10.0, CH_2), 3.02 (d, 2H, *J* 12.5, CH_2), 3.16 (t, 2H, *J* 6.5, CH_2), 7.56 (s, 1H, CONH), 7.87 (t, 1H, *J* 59.0, CHF_2), 8.02 (s, 1H), 8.34 (s, 1H), 8.44 (s, 1H), 8.50 (s, 1H) (total 4H, 2 × pyrazolyl-H & 2 × pyridinyl-H). **^{13}C NMR** (DMSO-d_6) δ 30.6, 31.8, 38.0, 41.3, 46.8, 110.5 (t, $J_{C\text{-}F}$ 247.0), 119.2, 124.9, 127.9, 128.0, 142.5, 149.3, 150.5, 152.6, 180.1 (two carbon signals overlapping or obscured). **HRMS** (ESI-TOF) 382.1234 [M(^{35}Cl)+H]$^+$ & 384.1217 [M(^{37}Cl)+H]$^+$; calcd. for $C_{17}H_{19}ClF_2N_5O^+$ 382.1241 [M(^{35}Cl)+H]$^+$ & 384.1211 [M(^{37}Cl)+H]$^+$. **Anal. RP-HPLC** Method C: t_R 15.04 min, purity >99%; Method D: t_R 10.72 min, purity >99%.

5-Bromo-4-chloropyridin-2-amine (34): To a suspension of 2-amino-4-chloropyridine (**33**, 7.72 g, 60.1 mmol) in anhydrous CH_3CN (120 mL) was added NBS (11.3 g, 63.5 mmol). The reaction mixture was stirred at room temperature under N_2 for 3 h and concentrated under reduced pressure. The residue was purified by flash column chromatography (DCM ramping to 4% CH_3OH in DCM) to give **34** as an orange solid (6.91 g, 58%). R_F (EtOAc:petroleum benzine = 1:1) 0.45. **^{1}H NMR** (DMSO-d_6) δ 6.42 (br s, 2H, NH_2), 6.67 (s, 1H, pyridinyl-H), 8.09 (s, 1H, pyridinyl-H). **^{13}C NMR** (DMSO-d_6) δ 104.6, 108.7, 142.3, 150.4, 159.9. **HRMS** (ESI-TOF) 206.9323, 208.9299 & 210.9268 [M+H]$^+$; calcd. for $C_5H_5BrClN_2^+$ 206.9320, 208.9299 & 210.9270 [M+H]$^+$.

5-Bromo-3,4-dichloropyridin-2-amine (35): To **34** (6.85 g, 33.0 mmol) in CH_3CN (125 mL) was added NCS (4.41 g, 33.0 mmol) in portions. The reaction mixture was heated at reflux under N_2 for 3 h, cooled down, and filtered. The solid was washed with CH_3CN (3 × 15 mL) and dried to give one portion of **35** as a tan powder (5.55 g). The filtrate and CH_3CN washings were combined and concentrated under reduced pressure, and the residue was purified by flash column chromatography (DCM ramping to 2% CH_3OH in DCM) to give a second portion of **35** as a beige solid (2.09 g) (total 7.64 g, 96%). R_F (DCM:CH_3OH = 98:2) 0.49. **^{1}H NMR** (DMSO-d_6) δ 6.83 (br s, 2H, NH_2), 8.12 (s, 1H, pyridinyl-H). **^{13}C NMR** (DMSO-d_6) δ 105.1, 112.1, 140.4, 147.8, 156.1. **HRMS** (ESI-TOF) 240.8929, 242.8905 & 244.8876 [M+H]$^+$; calcd. for $C_5H_4BrCl_2N_2^+$ 240.8930, 242.8909 & 244.8880 [M+H]$^+$.

5-Bromo-3,4-dichloro-*N*,*N*-bis(4-methoxybenzyl)pyridin-2-amine (36) & 5-bromo-3,4-dichloro-*N*-(4-methoxybenzyl)pyridin-2-amine (37): To a solution of amine **35** (2.42 g, 10.0 mmol) in anhydrous DMF (25 mL) on an ice-salt bath was added NaH (~60% suspension in mineral oil, 1.60 g, 40.0 mmol) in portions. The reaction mixture was stirred for 15 min, and a solution of 4-methoxybenzyl chloride (3.26 mL, 24.0 mmol) in anhydrous DMF (1 mL) was added. The reaction mixture was warmed up to room temperature, stirred for 2 h, quenched with saturated NH_4Cl aqueous solution (50 mL), and extracted with EtOAc (3 × 50 mL). The organic extracts were combined and concentrated under reduced pressure. The residue was purified by Biotage® FlashMaster Personal$^+$ flash chromatography (petroleum benzine ramping to 40% DCM in petroleum benzine) to give **36** as a colourless, clear oil (3.18 g, 66%) and **37** as a white solid (1.01 g, 28%). **36**: R_F (DCM:petroleum benzine = 2:1) 0.38. **^{1}H NMR** ($CDCl_3$) δ 3.79 (s, 6H, 2 × CH_3), 4.40 (s, 4H, 2 × CH_2), 6.83 (d, 4H, *J* 8.5, 4 × phenyl-H), 7.18 (d, 4H, *J* 8.5, 4 × phenyl-H), 8.24 (s, 1H, pyridinyl-H). **HRMS** (ESI-TOF) 481.0069, 483.0047 & 485.0020 [M+H]$^+$; calcd. for $C_{21}H_{20}BrCl_2N_2O_2^+$ 481.0080, 483.0060 & 485.0030 [M+H]$^+$. **37**: R_F (DCM:petroleum benzine = 2:1) 0.44. **^{1}H NMR** ($CDCl_3$) δ 3.80 (s, 3H, CH_3), 4.58 (d, 2H, *J* 5.0, CH_2), 5.34 (br s, 1H, NH), 6.88 (d, 2H, *J* 8.0, 2 × phenyl-H), 7.27 (d, 2H, *J* 8.0, 2 × phenyl-H), 8.16 (s, 1H, pyridinyl-H). **HRMS** (ESI-TOF) 360.9494, 362.9481 & 364.9442 [M+H]$^+$; calcd. for $C_{13}H_{12}BrCl_2N_2O^+$ 360.9505, 362.9485 & 364.9455 [M+H]$^+$.

8-(2-(Bis(4-methoxybenzyl)amino)-5-bromo-3-chloropyridin-4-yl)-2,8-diazaspiro[4.5]decan-1-one (38): Chloride **36** (3.24 g, 6.72 mmol) and *tert*-butyl 1-oxo-2,8-diazaspiro[4.5]

decane-8-carboxylate (1.71 g, 6.72 mmol) were coupled at 220 °C for 1 h according to general synthetic procedure B. The residue was purified by Biotage® FlashMaster Personal$^+$ flash chromatography (DCM ramping to 4% CH_3OH in DCM) to give **38** as a white foam (580 mg, 48%). R_F (DCM:CH_3OH = 97:3) 0.34. **^{1}H NMR** ($CDCl_3$) δ 1.51 (d, 2H, *J* 12.5, spiro-CH_2), 2.05–2.30 (m, 2H, spiro-CH_2), 2.17 (t, 2H, *J* 7.0, spiro-CH_2), 3.15–3.45 (m, 4H, spiro-CH_2), 3.38 (t, 2H, *J* 7.0, spiro-CH_2), 3.78 (s, 6H, 2 × CH_3), 4.35 (s, 4H, 2 × NCH_2-phenyl), 5.82 (br s, 1H, CONH), 6.81 (dd, 4H, *J* 8.5 & 3.0, 4 × phenyl-H), 7.18 (dd, 4H, *J* 8.5 & 2.0, 4 × phenyl-H), 8.13 (s, 1H, pyridinyl-H). **HRMS** (ESI-TOF) 599.1417 & 601.1409 $[M+H]^+$; calcd. for $C_{29}H_{33}BrClN_4O_3^+$ 599.1419 & 601.1399 $[M+H]^+$.

8-(5-Bromo-3-chloro-2-((4-methoxybenzyl)amino)pyridin-4-yl)-2,8-diazaspiro[4.5]decan-1-one (39): Chloride **37** (1.65 g, 4.58 mmol) and *tert*-butyl 1-oxo-2,8-diazaspiro[4.5]decane-8-carboxylate (1.28 g, 5.03 mmol) were coupled at 225 °C for 2.5 h according to general synthetic procedure B. The residue was purified by Biotage® FlashMaster Personal$^+$ flash chromatography (DCM ramping to 2% CH_3OH in DCM) to give **39** as a yellowish foam (1.48 g, 68%). R_F (DCM:CH_3OH = 97:3) 0.30. **^{1}H NMR** ($CDCl_3$) δ 1.50 (d, 2H, *J* 10.5, spiro-CH_2), 2.06–2.26 (m, 2H, spiro-CH_2), 2.16 (t, 2H, *J* 6.5, spiro-CH_2), 3.27 (app br s, 2H, spiro-CH_2) 3.29–3.36 (m, 2H, spiro-CH_2), 3.37 (t, 2H, *J* 6.5, spiro-CH_2), 3.80 (s, 3H, CH_3), 4.55 (d, 2H, *J* 4.5, NH*C*H_2-phenyl), 5.25 (br s, 1H), 5.66 (br s, 1H) (total 2H, CONH & CH_2–N*H*-pyridinyl), 6.88 (d, 2H, *J* 8.0, 2 × phenyl-H), 7.28 (d, 2H, *J* 8.5, 2 × phenyl-H), 8.06 (br s, 1H, pyridinyl-H). **HRMS** (ESI-TOF) 479.0838, 481.0825 & 483.0791 $[M+H]^+$; calcd. for $C_{21}H_{25}BrClN_4O_2^+$ 479.0844, 481.0824 & 483.0794 $[M+H]^+$.

8-(5-(Benzofuran-2-yl)-2-(bis(4-methoxybenzyl)amino)-3-chloropyridin-4-yl)-2,8-diazaspiro[4.5]decan-1-one (40): Bromide **38** (365 mg, 608 μmol) and 2-(benzofuran-2-yl)-4,4,5,5-tetramethyl-1,3,2-dioxaborolane (178 mg, 729 μmol) were reacted at 130 °C using general synthetic procedure A. The residue was purified by Biotage® FlashMaster Personal$^+$ flash chromatography (DCM ramping to 1.5% CH_3OH in DCM) to give **40** as a yellowish glue (170 mg, 44%). R_F (DCM:CH_3OH = 96:4) 0.44. **^{1}H NMR** ($CDCl_3$) δ 1.39 (d, 2H, *J* 12.5, spiro-CH_2), 2.04 (t, 2H, *J* 6.5, spiro-CH_2), 2.10 (app t, 2H, *J* 12.0, spiro-CH_2), 2.95 (t, 2H, *J* 11.0, spiro-CH_2), 3.23 (d, 2H, *J* 12.5, spiro-CH_2), 3.29 (t, 2H, *J* 11.0, spiro-CH_2), 3.79 (s, 6H, 2 × CH_3), 4.47 (s, 4H, 2 × NCH_2-phenyl), 5.55 (br s, 1H, CONH), 6.83 (d, 4H, *J* 8.0, 4 × phenyl-H), 6.84 (s, 1H, benzofuranyl-H), 7.21 (d, 4H, *J* 8.0, 4 × phenyl-H), 7.24–7.35 (m, 2H, 2 × benzofuranyl-H), 7.52 (d, 1H, *J* 8.0, benzofuranyl-H), 7.63 (d, 1H, *J* 6.5, benzofuranyl-H), 8.24 (s, 1H, pyridinyl-H). **^{13}C NMR** ($CDCl_3$) δ 32.3, 38.7, 41.9, 46.5, 53.2, 55.4, 104.1, 111.2, 113.8, 117.0, 118.6, 121.2, 123.1, 124.3, 129.4, 129.5, 130.8, 147.6, 153.7, 155.0, 155.6, 158.7, 160.5, 181.6 (thirteen carbon signals overlapping or obscured). **HRMS** (ESI-TOF) 637.2575, 638.2596 & 639.2553 $[M+H]^+$; calcd. for $C_{37}H_{38}ClN_4O_4^+$ 637.2577, 638.2610 & 639.2547 $[M+H]^+$.

8-(5-(Benzo[*b*]thiophen-2-yl)-3-chloro-2-((4-methoxybenzyl)amino)pyridin-4-yl)-2,8-diazaspiro[4.5]decan-1-one (41): Bromide **39** (288 mg, 600 μmol) and benzo[*b*]thiophen-2-ylboronic acid (128 mg, 719 μmol) were reacted at 130 °C using general synthetic procedure A. The residue was purified by Biotage® FlashMaster Personal$^+$ flash chromatography (DCM ramping to 2% CH_3OH in DCM) to give **41** as a yellowish foam (145 mg, 45%). R_F (DCM:CH_3OH = 94:6) 0.61. **^{1}H NMR** ($CDCl_3$) δ 1.37 (d, 2H, *J* 13.0, spiro-CH_2), 2.03 (t, 2H, *J* 6.5, spiro-CH_2), 2.10 (td, 2H, *J* 11.5 & 3.5, spiro-CH_2), 3.03 (app br s, 2H, spiro-CH_2), 3.21 (d, 2H, *J* 12.0, spiro-CH_2), 3.28 (t, 2H, *J* 6.5, spiro-CH_2), 3.81 (s, 3H, CH_3), 4.64 (d, 2H, *J* 5.0, NH*C*H_2-phenyl), 5.40 (t, 1H, *J* 4.5, CH_2–N*H*-pyridinyl), 5.54 (br s, 1H, CONH), 6.90 (d, 2H, *J* 8.0, 2 × phenyl-H), 7.24 (s, 1H, benzothiophenyl-H), 7.32 (d, 2H, *J* 8.0, 2 × phenyl-H), 7.27–7.42 (m, 2H, 2 × benzothiophenyl-H), 7.79 (d, 1H, *J* 7.5, benzothiophenyl-H), 7.85 (d, 1H, *J* 7.5, benzothiophenyl-H), 8.10 (s, 1H, pyridinyl-H). **^{13}C NMR** ($CDCl_3$) δ 31.2, 32.2, 38.7, 42.0, 45.5, 46.8, 55.5, 114.2, 122.3, 122.4, 123.4, 124.2, 124.5, 129.2, 131.5, 140.1, 140.7, 148.4, 153.8, 155.3, 159.1, 181.7 (seven carbon signals overlapping or obscured). **HRMS** (ESI-TOF) 533.1782, 534.1796 & 535.1754 $[M+H]^+$; calcd. for $C_{29}H_{30}ClN_4O_2S^+$ 533.1773, 534.1807 & 535.1743 $[M+H]^+$.

8-(2-Amino-5-(benzofuran-2-yl)-3-chloropyridin-4-yl)-2,8-diazaspiro[4.5]decan-1-one (42): Compound **40** (166 mg, 260 μmol) was de-protected using general synthetic procedure C. The residue was purified by Biotage® FlashMaster Personal$^+$ flash chromatography (DCM ramping to 5% CH_3OH in DCM), and crystallised with CH_3OH/DCM/EtOAc to give **42** as a white solid (77 mg, 75%). R_F (DCM:CH_3OH = 94:6) 0.32. **m.p.** 234–235 °C. **^{1}H NMR** (DMSO-d_6) δ 1.28 (app d, 2H, *J* 12.5, CH_2), 1.77 (td, 2H, *J* 11.5 & 1.5, CH_2), 1.86 (t, 2H, *J* 6.5, CH_2), 2.81 (t, 2H, *J* 11.0, CH_2), 3.02 (d, 2H, *J* 12.0, CH_2), 3.12 (t, 2H, *J* 6.0, CH_2), 6.48 (s, 2H, NH_2), 6.98 (s, 1H, benzofuranyl-H), 7.25 (t, 1H, *J* 7.5, benzofuranyl-H), 7.30 (t, 1H, *J* 7.0, benzofuranyl-H), 7.53 (s, 1H, CONH), 7.59 (d, 1H, *J* 8.0, benzofuranyl-H), 7.64 (d, 1H, *J* 7.0, benzofuranyl-H), 8.00 (s, 1H, pyridinyl-H). **^{13}C NMR** (DMSO-d_6) δ 30.2, 31.9, 38.0, 41.6, 46.0, 103.6, 109.3, 111.1, 112.9, 121.0, 123.1, 124.2, 129.1, 148.6, 153.8, 154.1, 154.3, 157.7, 180.3 (two carbon signals overlapping or obscured). **HRMS** (ESI-TOF) 397.1421 $[M(^{35}Cl)+H]^+$ & 399.1426 $[M(^{37}Cl)+H]^+$; calcd. for $C_{21}H_{22}ClN_4O_2^+$ 397.1426 $[M(^{35}Cl)+H]^+$ & 399.1396 $[M(^{37}Cl)+H]^+$. **Anal. RP-HPLC** Method C: t_R 17.51 min, purity >97%; Method D: t_R 12.46 min, purity >97%.

8-(2-Amino-5-(benzo[*b*]thiophen-2-yl)-3-chloropyridin-4-yl)-2,8-diazaspiro[4.5]decan-1-one (43): Compound **41** (140 mg, 263 μmol) was de-protected using general synthetic procedure C. The residue was purified by Biotage® FlashMaster Personal$^+$ flash chromatography (DCM ramping to 3.5% CH_3OH in DCM), and crystallised with CH_3OH/DCM/EtOAc to give **43** as a white solid (66 mg, 61%). R_F (DCM:CH_3OH = 94:6) 0.38. **m.p.** 264–265 °C. **^{1}H NMR** (DMSO-d_6) δ 1.28 (app d, 2H, *J* 12.5, CH_2), 1.75–2.05 (m, 4H, 2 × CH_2), 3.04 (app s, 4H, 2 × CH_2), 3.12 (t, 2H, *J* 6.0, CH_2), 6.39 (s, 2H, NH_2), 7.33 (t, 1H, *J* 7.5, benzothiophenyl-H), 7.37 (t, 1H, *J* 7.5, benzothiophenyl-H), 7.44 (br s, 1H), 7.52 (s, 1H) (total 2H, CONH & benzothiophenyl-H), 7.82 (d, 1H, *J* 7.5, benzothiophenyl-H), 7.93 (d, 1H, *J* 7.5, benzothiophenyl-H), 8.00 (br s, 1H, pyridinyl-H). **^{13}C NMR** (DMSO-d_6) δ 30.3, 31.5, 38.0, 41.5, 46.3, 122.2, 123.5, 124.3, 124.6, 139.7, 139.9, 148.2, 153.5, 157.3, 180.3 (six carbon signals overlapping or obscured). **HRMS** (ESI-TOF) 413.1195 $[M(^{35}Cl)+H]^+$ & 415.1165 $[M(^{37}Cl)+H]^+$; calcd. for $C_{21}H_{22}ClN_4OS^+$ 413.1197 $[M(^{35}Cl)+H]^+$ & 415.1168 $[M(^{37}Cl)+H]^+$. **Anal. RP-HPLC** Method C: t_R 17.66 min, purity >98%; Method D: t_R 12.59 min, purity >99%.

1-Methyl-5-(4,4,5,5-tetramethyl-1,3,2-dioxaborolan-2-yl)-1*H*-indazole (44): To a suspension of 5-bromo-1-methyl-1*H*-indazole (2.11 g, 10.0 mmol) and 4,4,4′,4′,5,5,5′,5′-octamethyl-2,2′-bi(1,3,2-dioxaborolane) (3.81 g, 15.0 mmol) in DMSO (25 mL) were added potassium acetate (2.95 g, 30.1 mmol) and Pd(dppf)$Cl_2 \cdot CH_2Cl_2$ (409 mg, 501 μmol). The reaction mixture was degassed with N_2, heated at 80 °C for 20 h, cooled down, and partitioned between distilled H_2O (200 mL) and EtOAc (200 mL). The mixture was filtered through a pad of Celite®, and the solids were washed with EtOAc (100 mL). The filtrate and washing were combined, and the organic layer was separated. The aqueous layer was extracted with EtOAc (2 × 100 mL). The organic layer and extracts were combined, dried over Na_2SO_4, and concentrated under reduced pressure. The residue was purified by Biotage® FlashMaster Personal$^+$ flash chromatography (petroleum benzine ramping to 2% CH_3OH in DCM) to give **44** as a white solid (1.68 g, 65%). R_F (DCM) 0.21. **^{1}H NMR** ($CDCl_3$) δ 1.37 (s, 12H, 4 × dioxaborolanyl-CH_3), 4.07 (s, 3H, NCH_3), 7.37 (dt, 1H, *J* 8.5 & 1.0, indazolyl-H), 7.80 (dd, 1H, *J* 8.5 & 0.5, indazolyl-H), 7.99 (d, 1H, *J* 0.5, indazolyl-H), 8.26 (s, 1H, indazolyl-H). **^{13}C NMR** ($CDCl_3$) δ 25.0, 35.6, 83.9, 108.3, 124.1, 129.6, 131.9, 133.7, 141.5 (five carbon signals overlapping or obscured).

HRMS (ESI-TOF) 259.1613 $[M+H]^+$; calcd. for $C_{14}H_{20}BN_2O_2^+$ 259.1613 $[M+H]^+$.

8-(2-(Bis(4-methoxybenzyl)amino)-3-chloro-5-(1-methyl-1*H*-indazol-5-yl)pyridin-4-yl)-2,8-diazaspiro[4.5]decan-1-one (45): Bromide **38** (510 mg, 850 μmol) and boronate ester **44** (230 mg, 891 μmol) were reacted at 120 °C using general synthetic procedure A. The residue was purified by Biotage® FlashMaster Personal$^+$ flash chromatography (DCM ramping to DCM/EtOAc/EtOH = 50:45:5) to give **45** as a yellowish glue (90 mg, 16%). R_F (DCM:EtOAc:EtOH = 50:46:4) 0.17. **^{1}H NMR** ($CDCl_3$) δ 1.29 (d, 2H, *J* 13.0, spiro-CH_2), 1.93 (t, 4H, *J* 7.0, 2 × spiro-CH_2), 2.74 (app br s, 2H, spiro-CH_2), 3.12 (dt, 2H, *J* 12.5 & 1.0, spiro-CH_2), 3.24 (t, 2H, *J* 7.0, spiro-CH_2), 3.79 (s, 6H, 2 × OCH_3), 4.12 (s, 3H, NCH_3), 4.43 (s, 4H, 2 × NCH_2-phenyl), 5.49 (br s, 1H, CONH), 6.84 (d, 4H, *J* 8.5, 4 × phenyl-H), 7.25 (d, 4H, *J* 8.0, 4 × phenyl-H), 7.33 (d, 1H, *J* 8.5, indazolyl-H), 7.46 (d, 1H, *J* 8.5, indazolyl-H), 7.61 (s, 1H, indazolyl-H), 7.96 (s, 1H), 8.02 (s, 1H) (total 2H, indazolyl-H & pyridinyl-H). **HRMS** (ESI-TOF) 651.2851, 652.2893 & 653.2840 $[M+H]^+$; calcd. for $C_{37}H_{40}ClN_6O_3^+$ 651.2845, 652.2879 & 653.2816 $[M+H]^+$.

8-(2-Amino-3-chloro-5-(1-methyl-1*H*-indazol-5-yl)pyridin-4-yl)-2,8-diazaspiro[4.5]decan-1-one (CCT251921): Compound **45** (80 mg, 0.12 mmol) was de-protected using general synthetic procedure C. The residue was purified by Biotage® FlashMaster Personal$^+$ flash chromatography (DCM ramping to 7% CH_3OH in DCM), and washed with EtOAc (10 mL) to give CCT251921 as a white solid (44 mg, 88%). R_F (DCM:CH_3OH = 94:6) 0.34. **m.p.** 266–267 °C. **^{1}H NMR** (DMSO-d_6) δ 1.16 (app d, 2H, *J* 13.0, CH_2), 1.65 (app t, 2H, *J* 10.0, CH_2), 1.75 (t, 2H, *J* 7.0, CH_2), 2.60 (app br s, 2H, CH_2), 2.95 (app d, 2H, *J* 12.5, CH_2), 3.06 (t, 2H, *J* 7.0, CH_2), 4.06 (s, 3H, CH_3), 6.07 (s, 2H, NH_2), 7.27 (dd, 1H, *J* 8.5 & 1.5, indazolyl-H), 7.47 (s, 1H, CONH), 7.62 (s, 1H, indazolyl-H), 7.65 (s, 1H, indazolyl-H), 7.65 (d, 1H, *J* 8.5, indazolyl-H), 8.05 (s, 1H, pyridinyl-H). **^{13}C NMR** (DMSO-d_6) δ 30.3, 31.9, 35.5, 37.9, 41.5, 47.4, 108.9, 109.3, 120.4, 123.8, 124.3, 128.5, 130.7, 132.6, 138.8, 148.2, 153.7, 156.3, 180.2 (two carbon signals overlapping or obscured). **HRMS** (ESI-TOF) 411.1695 $[M(^{35}Cl)+H]^+$ & 413.1674 $[M(^{37}Cl)+H]^+$; calcd. for $C_{21}H_{24}ClN_6O^+$ 411.1695 $[M(^{35}Cl)+H]^+$ & 413.1665 $[M(^{37}Cl)+H]^+$. **Anal. RP-HPLC** Method A: t_R 9.12 min, purity >95%; Method B: t_R 7.82 min, purity >98%.

4.3. Biology

4.3.1. Kinase assays

At ProQinase GmbH, the ^{33}PanQinase® activity assay, a radiometric protein kinase assay, was used to measure the residual kinase activity of CDK8/cyclin C. The assay was performed in a 96-well FlashPlate™ from PerkinElmer (Boston, MA, USA) in a reaction volume of 50 μL on a Beckman Coulter/SAGIAN™ Core System. A reaction cocktail was formed by pipetting the following four solutions in an order of [i] 20 μL of assay buffer (standard buffer), [ii] 5 μL of ATP solution (in H_2O), [iii] 5 μL of a test compound (in 10% DMSO) [iv] 10 μL of enzyme (*i.e.*, CDK8), solution & 10 μL of substrate (*i.e.*, RBER-IRStide) solution (premixed). Each well contained 70 mM HEPES-NaOH pH 7.5, 3 mM $MgCl_2$, 3 mM $MnCl_2$, 3 μM sodium orthovanadate, 1.2 mM dithiothreitol (DTT), 50 μg/mL polyethylene glycol (PEG) 20000, 1.0 μM ATP (the concentration corresponds to the apparent K_m (ATP) value of CDK8), [γ-^{33}P]-ATP (4-9 × 10^5 cpm per well), 1 ng/μL CDK8 (ProQinase lot: 004), and 20 ng/μL RBER-IRStide (ProQinase lot: 019 or 023). The reaction cocktails were incubated at 30 °C for 60 min. The reactions were stopped with addition of 50 μL of 2% (v/v) H_3PO_4, and plates aspirated and washed twice with 200 μL of 0.9% (w/v) NaCl. Incorporation of $^{33}P_i$ was determined with a microplate scintillation counter (Microbeta, Wallace). A residual kinase activity (%) at each compound concentration and an IC_{50} value of a test compound were calculated using Quattro Workflow V3.1.1 (Quattro Research GmbH, Münich, Germany; www.quattro-research.com/). The fitting model used for the IC_{50} determination was sigmoidal dose-response (variable slope) with the parameters of TOP and BOTTOM fixed at 100% and 0%, respectively. The method of least squares was used for regression analysis. Percentages of residual kinase activity of the kinases (except CDK8) in the preliminary screening in the presence of 1 μM **19** or **42** and in the near-kinome-wide profiling with 1 μM **42**, and IC_{50} values of **42** against LRRK2, FMS and FLT3 were measured using the HotSpot™ radioisotope-based kinase assay at Reaction Biology Corporation (the assay protocol is available at https://www.reactionbiology.com/services/target-specific-assays/kinase-assays/kinase-screening). All the IC_{50} values determined by two contract research organisations were converted to K_i values using the Cheng-Prusoff equation: $K_i = IC_{50}/(1 + ([ATP]/K_m(ATP)))$, where [ATP] is the concentration of ATP used for the IC_{50} determination and K_m (ATP) for each kinase is determined experimentally [83].

4.3.2. Cell culture

All the cell lines were obtained from the cell bank at Drug Discovery and Development, University of South Australia. Each of them was cultured, according to the American Type Culture Collection (ATCC) recommendation, in Roswell Park Memorial Institute (RPMI)-1640, Dulbecco's Modified Eagle's Medium (DMEM), or Minimum Essential Media (MEM), with 10% foetal bovine serum (FBS, Sigma-Aldrich, Castle Hill, NSW, Australia) within a humidified incubator at 37 °C in the presence of 5% CO_2. No mycoplasma contamination [84] was detected in cell culture.

4.3.3. Cell viability assays

MTT (Life Technologies, Mulgrave, Vic, Australia) and resazurin (Sigma-Aldrich) assays were performed with adherent (solid tumour) and suspension (leukaemia) cell lines, respectively, as reported previously [44,64]. Compound concentrations required to inhibit 50% of cell growth (GI_{50}) were calculated using nonlinear regression analysis.

4.3.4. Determination of in vivo pharmacokinetic properties

Healthy male Sprague-Dawley rats (250–350 g) or male adult BALB/c mice (20–25 g) were allocated into IV- and PO-dosing groups; n = 3 per group for rats, and n = 10 per group for mice. Rodents were administered an IV injection of **42** or **43** *via* the tail vein (5 mg/kg for rats, and 2 mg/kg for mice), or a single oral dose by gavage (20 mg/kg for rats, and 10 mg/kg for mice; 2-h prior fasting was fulfilled). IV formulations consisted of **42** or **43** dissolved in a mixture of 0.1 M sodium acetate buffer (pH 4.5):PEG 400:DMSO (9:9:2, v/v/v), and oral formulations were comprised of **42** or **43** dispersed in 1% (w/v) carboxymethyl cellulose aqueous solution. Blood samples were collected from animals by jugular vein cannula (rats) or cheek bleeding and cardiac puncture under anaesthesia (mice) at time zero and at intervals up to 24 h. Collected blood samples were centrifuged at 7000 *g* for 3 min to separate plasma samples which were stored at −20 °C until analysis. Concentrations of **42** or **43** in plasma samples were quantified using a validated LC/MS/MS method with the AB SCIEX TripleTOF 5600 mass spectrometer. Briefly, plasma samples were supplemented with an internal standard (IS) and extracted with EtOAc, and organic phases separated and dried in a Genevac HT-4X HCL centrifugal vacuum evaporator (SP Scientific, Ipswich, UK). The residues were reconstituted in acetonitrile/water (50:50), injected into a Shimadzu Nexera HPLC system, and resolved on a Phenomenex Kinetex Biphenyl column (1.7 μm, 100 Å, 50 mm × 2.1 mm) at a mobile phase flow rate of 0.5 mL/min. Mobile phase A was 5% methanol and 0.1% FA in water, and mobile phase B (MPB) 95%

methanol and 0.1% FA in water. The mobile phase timetable was set as a linear gradient starting from 2% MPB for 0.5 min, followed by ramping to 100% MPB over 2.3 min and maintaining at 100% MPB for 1.5 min before returning to 2% MPB for 0.5 min in preparation for the next sample. Ratios of signal areas of compound/IS were obtained from known concentrations of calibrators and were used to construct a calibration curve which was used to determine the plasma concentrations of unknown samples. The limit of quantification was 5 ng/mL. The intraday and interday variability for each compound was within ±15%. Non-compartmental analyses of plasma concentration versus time were performed using Phoenix WinNonlin (Certara, St. Louis, MO, USA). These experiments were carried out under the approval of the University of South Australia Animal Ethics Committee (Animal Ethics Number: U21-16).

4.3.5. Evaluation of in vitro drug-like properties

All of the assays were performed with **42** at Cyprotex Discovery Ltd. (Macclesfield, UK), and experimental details can be found at https://www.cyprotex.com/services. Briefly, Log $D_{7.4}$ was assessed using the shake flask assay with a buffer at pH 7.4, and pKa acquired with a fast UV spectrometric titration. Aqueous solubility was estimated by turbidimetry. Bidirectional permeability was measured using Caco-2 cell line. Inhibition of CYP450 enzymes and the hERG potassium channel was gauged using human liver microsomes and CHO-hERG cells, respectively.

4.3.6. Western blot analysis

Western blotting was performed as described previously [85]. Primary antibodies included STAT1, STAT1 with phosphorylated S727 (p-STAT1^{S727}), Rb with phosphorylated S780 (p-Rb^{S780}), Mcl-1 and β-actin (Cell Signaling Technology, Danvers, MA, USA). The anti-rabbit immunoglobulin G (IgG) horseradish peroxidase-conjugated antibody (Cell Signaling Technology) was used as a secondary antibody. Enhanced Chemiluminescence reagents (GE Healthcare Life Sciences, Rydalmere, NSW, Australia) were used for western blot detection.

4.3.7. Cell cycle analysis and apoptosis detection

Cell cycle analysis and apoptosis detection were performed with flow cytometry as described previously [86]. Briefly, MV4-11 cells were seeded at 8×10^4 and incubated at 37 °C, 5% CO_2 overnight. After incubation with **42** for 72 h, cell pellets were collected and centrifuged (300 *g*, 5 min). For cell cycle analysis, cell pellets were fixed with 70% ethanol on ice for 15 min and collected again. The collected pellets were incubated with a PI staining solution (50 mg/mL PI, 0.1 mg/mL RNase A and 0.05% Triton™ X-100) at room temperature for 1 h and analysed by a Gallios flow cytometer (Beckman Coulter, Brea, CA, USA). Apoptosis detection was carried out with an FITC annexin-V/PI commercial kit (Becton Dickinson, Franklin Lakes, NJ, USA) following the manufacturer protocol. The samples were analysed by fluorescence-activated cell sorting using the Gallios flow cytometer within 1 h after staining. Data were analysed using Kaluza v1.2 (Beckman Coulter).

Declaration of competing interest

The authors declare that they have no known competing financial interests or personal relationships that could have appeared to influence the work reported in this paper.

Acknowledgements

This work was supported by a grant from Yabao Pharmaceutical Group Co., Ltd., China to S.W..

Appendix A. Supplementary data

Supplementary data to this article can be found online at https://doi.org/10.1016/j.ejmech.2021.113391.

References

[1] I. Menzl, A. Witalisz-Siepracka, V. Sexl, CDK8-novel therapeutic opportunities, Pharmaceuticals 12 (2019) 92–103.
[2] S. Philip, M. Kumarasiri, T. Teo, M. Yu, S. Wang, Cyclin-dependent kinase 8: a new hope in targeted cancer therapy? J. Med. Chem. 61 (2018) 5073–5092.
[3] J. Bancerek, Z.C. Poss, I. Steinparzer, V. Sedlyarov, T. Pfaffenwimmer, I. Mikulic, L. Dolken, B. Strobl, M. Muller, D.J. Taatjes, P. Kovarik, CDK8 kinase phosphorylates transcription factor STAT1 to selectively regulate the interferon response, Immunity 38 (2013) 250–262.
[4] C.J. Fryer, J.B. White, K.A. Jones, Mastermind recruits CycC:CDK8 to phosphorylate the Notch ICD and coordinate activation with turnover, Mol. Cell 16 (2004) 509–520.
[5] C. Alarcón, A.-I. Zaromytidou, Q. Xi, S. Gao, J. Yu, S. Fujisawa, A. Barlas, A.N. Miller, K. Manova-Todorova, M.J. Macias, G. Sapkota, D. Pan, J. Massagué, Nuclear CDKs drive Smad transcriptional activation and turnover in BMP and TGF-β pathways, Cell 139 (2009) 757–769.
[6] A.D. Clark, M. Oldenbroek, T.G. Boyer, Mediator kinase module and human tumorigenesis, Crit. Rev. Biochem. Mol. Biol. 50 (2015) 393–426.
[7] B.L. Allen, D.J. Taatjes, The Mediator complex: a central integrator of transcription, Nat. Rev. Mol. Cell Biol. 16 (2015) 155–166.
[8] R.C. Conaway, S. Sato, C. Tomomori-Sato, T. Yao, J.W. Conaway, The mammalian Mediator complex and its role in transcriptional regulation, Trends Biochem. Sci. 30 (2005) 250–255.
[9] Z. Szilagyi, C.M. Gustafsson, Emerging roles of Cdk8 in cell cycle control, Biochim. Biophys. Acta Gene Regul. Mech. 1829 (2013) 916–920.
[10] A. Nakamura, D. Nakata, Y. Kakoi, M. Kunitomo, S. Murai, S. Ebara, A. Hata, T. Hara, CDK8/19 inhibition induces premature G1/S transition and ATR-dependent cell death in prostate cancer cells, Oncotarget 9 (2018) 13474–13487.
[11] D. Xu, C.F. Li, X. Zhang, Z. Gong, C.H. Chan, S.W. Lee, G. Jin, A.H. Rezaeian, F. Han, J. Wang, W.L. Yang, Z.Z. Feng, W. Chen, C.Y. Wu, Y.J. Wang, L.P. Chow, X.F. Zhu, Y.X. Zeng, H.K. Lin, Skp2-macroH2A1-CDK8 axis orchestrates G2/M transition and tumorigenesis, Nat. Commun. 6 (2015). Article number: 6641.
[12] R. Firestein, A.J. Bass, S.Y. Kim, I.F. Dunn, S.J. Silver, I. Guney, E. Freed, A.H. Ligon, N. Vena, S. Ogino, M.G. Chheda, P. Tamayo, S. Finn, Y. Shrestha, J.S. Boehm, S. Jain, E. Bojarski, C. Mermel, J. Barretina, J.A. Chan, J. Baselga, J. Tabernero, D.E. Root, C.S. Fuchs, M. Loda, R.A. Shivdasani, M. Meyerson, W.C. Hahn, CDK8 is a colorectal cancer oncogene that regulates β-catenin activity, Nature 455 (2008) 547–551.
[13] A. Kapoor, M.S. Goldberg, L.K. Cumberland, K. Ratnakumar, M.F. Segura, P.O. Emanuel, S. Menendez, C. Vardabasso, G. Leroy, C.I. Vidal, D. Polsky, I. Osman, B.A. Garcia, E. Hernando, E. Bernstein, The histone variant macroH2A suppresses melanoma progression through regulation of CDK8, Nature 468 (2010) 1105–1109.
[14] H.E. Pelish, B.B. Liau, I.I. Nitulescu, A. Tangpeerachaikul, Z.C. Poss, D.H. Da Silva, B.T. Caruso, A. Arefolov, O. Fadeyi, A.L. Christie, K. Du, D. Banka, E.V. Schneider, A. Jestel, G. Zou, C. Si, C.C. Ebmeier, R.T. Bronson, A.V. Krivtsov, A.G. Myers, N.E. Kohl, A.L. Kung, S.A. Armstrong, M.E. Lemieux, D.J. Taatjes, M.D. Shair, Mediator kinase inhibition further activates super-enhancer-associated genes in AML, Nature 526 (2015) 273–276.
[15] W. Xu, Z. Wang, W. Zhang, K. Qian, H. Li, D. Kong, Y. Li, Y. Tang, Mutated K-ras activates CDK8 to stimulate the epithelial-to-mesenchymal transition in pancreatic cancer in part via the Wnt/β-catenin signaling pathway, Canc. Lett. 356 (2015) 613–627.
[16] J. Brägelmann, N. Klümper, A. Offermann, A. von Mässenhausen, D. Böhm, M. Deng, A. Queisser, C. Sanders, I. Syring, A.S. Merseburger, W. Vogel, E. Sievers, I. Vlasic, J. Carlsson, O. Andrén, P. Brossart, S. Duensing, M.A. Svensson, Z. Shaikhibrahim, J. Kirfel, S. Perner, Pan-cancer analysis of the Mediator complex transcriptome identifies CDK19 and CDK8 as therapeutic targets in advanced prostate cancer, Clin. Canc. Res. 23 (2017) 1829–1840.
[17] I.B. Roninson, B. Győrffy, Z.T. Mack, A.A. Shtil, M.S. Shtutman, M. Chen, E.V. Broude, Identifying cancers impacted by CDK8/19, Cells 8 (2019) 821–836.
[18] X.Y. Li, Q.F. Luo, C.K. Wei, D.F. Li, J. Li, L. Fang, MiRNA-107 inhibits proliferation and migration by targeting CDK8 in breast cancer, Int. J. Clin. Exp. Med. 7 (2014) 32–40.
[19] X.Y. Li, Q.F. Luo, C.K. Wei, D.F. Li, L. Fang, siRNA-mediated silencing of CDK8 inhibits proliferation and growth in breast cancer cells, Int. J. Clin. Exp. Pathol. 7 (2014) 92–100.
[20] J. Li, X. Li, X. Kong, Q. Luo, J. Zhang, L. Fang, MiRNA-26b inhibits cellular proliferation by targeting CDK8 in breast cancer, Int. J. Clin. Exp. Med. 7 (2014) 558–565.
[21] J. Liang, M. Chen, D. Hughes, A.A. Chumanevich, S. Altilia, V. Kaza, C.U. Lim, H. Kiaris, K. Mythreye, M.M. Pena, E.V. Broude, I.B. Roninson, CDK8 selectively promotes the growth of colon cancer metastases in the liver by regulating gene expression of TIMP3 and matrix metalloproteinases, Canc. Res. 78 (2018) 6594–6606.

[22] P. Czodrowski, A. Mallinger, D. Wienke, C. Esdar, O. Poschke, M. Busch, F. Rohdich, S.A. Eccles, M.J. Ortiz-Ruiz, R. Schneider, F.I. Raynaud, P.A. Clarke, D. Musil, D. Schwarz, T. Dale, K. Urbahns, J. Blagg, K. Schiemann, Structure-based optimization of potent, selective, and orally bioavailable CDK8 Inhibitors discovered by high-throughput screening, J. Med. Chem. 59 (2016) 9337–9349.
[23] A. Mallinger, K. Schiemann, C. Rink, F. Stieber, M. Calderini, S. Crumpler, M. Stubbs, O. Adeniji-Popoola, O. Poeschke, M. Busch, P. Czodrowski, D. Musil, D. Schwarz, M.-J. Ortiz-Ruiz, R. Schneider, C. Thai, M. Valenti, A. de Haven Brandon, R. Burke, P. Workman, T. Dale, D. Wienke, P.A. Clarke, C. Esdar, F.I. Raynaud, S.A. Eccles, F. Rohdich, J. Blagg, Discovery of potent, selective, and orally bioavailable small-molecule modulators of the Mediator complex-associated kinases CDK8 and CDK19, J. Med. Chem. 59 (2016) 1078–1101.
[24] P.A. Clarke, M.J. Ortiz-Ruiz, R. TePoele, O. Adeniji-Popoola, G. Box, W. Court, S. Czasch, S. El Bawab, C. Esdar, K. Ewan, S. Gowan, A. De Haven Brandon, P. Hewitt, S.M. Hobbs, W. Kaufmann, A. Mallinger, F. Raynaud, T. Roe, F. Rohdich, K. Schiemann, S. Simon, R. Schneider, M. Valenti, S. Weigt, J. Blagg, A. Blaukat, T.C. Dale, S.A. Eccles, S. Hecht, K. Urbahns, P. Workman, D. Wienke, Assessing the mechanism and therapeutic potential of modulators of the human Mediator complex-associated protein kinases, Elife 5 (2016), e20722.
[25] A. Mallinger, S. Crumpler, M. Pichowicz, D. Waalboer, M. Stubbs, O. Adeniji-Popoola, B. Wood, E. Smith, C. Thai, A.T. Henley, K. Georgi, W. Court, S. Hobbs, G. Box, M.-J. Ortiz-Ruiz, M. Valenti, A. De Haven Brandon, R. TePoele, B. Leuthner, P. Workman, W. Aherne, O. Poeschke, T. Dale, D. Wienke, C. Esdar, F. Rohdich, F. Raynaud, P.A. Clarke, S.A. Eccles, F. Stieber, K. Schiemann, J. Blagg, Discovery of potent, orally bioavailable, small-molecule inhibitors of WNT signaling from a cell-based pathway screen, J. Med. Chem. 58 (2015) 1717–1735.
[26] D. Kim, C.Y. Wang, R. Hu, J.Y. Lee, T.T. Luu, H.J. Park, S.K. Lee, Antitumor activity of vanicoside B isolated from persicaria dissitiflora by targeting CDK8 in triple-negative breast cancer cells, J. Nat. Prod. 82 (2019) 3140–3149.
[27] M.S. McDermott, A.A. Chumanevich, C.U. Lim, J. Liang, M. Chen, S. Altilia, D. Oliver, J.M. Rae, M. Shtutman, H. Kiaris, B. Gyorffy, I.B. Roninson, E.V. Broude, Inhibition of CDK8 mediator kinase suppresses estrogen dependent transcription and the growth of estrogen receptor positive breast cancer, Oncotarget 8 (2017), 12588-12575.
[28] T. Rzymski, M. Mikula, E. Zylkiewicz, A. Dreas, K. Wiklik, A. Golas, K. Wojcik, M. Masiejczyk, A. Wrobel, I. Dolata, A. Kitlinska, M. Statkiewicz, U. Kuklinska, K. Goryca, L. Sapala, A. Grochowska, A. Cabaj, M. Szajewska-Skuta, E. Gabor-Worwa, K. Kucwaj, A. Bialas, A. Radzimierski, M. Combik, J. Woyciechowski, M. Mikulski, R. Windak, J. Ostrowski, K. Brzozka, SEL120-34A is a novel CDK8 inhibitor active in AML cells with high levels of serine phosphorylation of STAT1 and STAT5 transactivation domains, Oncotarget 8 (2017) 33779–33795.
[29] K. Ono, H. Banno, M. Okaniwa, T. Hirayama, N. Iwamura, Y. Hikichi, S. Murai, M. Hasegawa, Y. Hasegawa, K. Yonemori, A. Hata, K. Aoyama, D.R. Cary, Design and synthesis of selective CDK8/19 dual inhibitors: discovery of 4,5-dihydrothieno[3',4':3,4]benzo[1,2-d]isothiazole derivatives, Bioorg, Med. Chem. Lett. 25 (2017) 2336–2350.
[30] J. Fujimoto, T. Hirayama, Y. Hirata, Y. Hikichi, S. Murai, M. Hasegawa, Y. Hasegawa, K. Yonemori, A. Hata, K. Aoyama, D.R. Cary, Studies of CDK 8/19 inhibitors: discovery of novel and selective CDK8/19 dual inhibitors and elimination of their CYP3A4 time-dependent inhibition potential, Bioorg. Med. Chem. 25 (2017) 3018–3033.
[31] M.H. Hofmann, R. Mani, H. Engelhardt, M.A. Impagnatiello, S. Carotta, M. Kerenyi, S. Lorenzo-Herrero, J. Böttcher, D. Scharn, H. Arnhof, A. Zoephel, R. Schnitzer, T. Gerstberger, M.P. Sanderson, G. Rajgolikar, S. Goswami, S. Vasu, P. Ettmayer, S. Gonzalez, M. Pearson, D.B. McConnell, N. Kraut, N. Muthusamy, J. Moll, Selective and potent CDK8/19 inhibitors enhance NK-cell activity and promote tumor surveillance, Mol. Canc. Therapeut. 19 (2020) 1018–1030.
[32] S. Aoki, Y. Watanabe, M. Sanagawa, A. Setiawan, N. Kotoku, M. Kobayashi, Cortistatins A, B, C, and D, anti-angiogenic steroidal alkaloids, from the marine sponge corticium simplex, J. Am. Chem. Soc. 128 (2006) 3148–3149.
[33] V.J. Cee, D.Y. Chen, M.R. Lee, K.C. Nicolaou, Cortistatin A is a high-affinity ligand of protein kinases ROCK, CDK8, and CDK11, Angew. Chem. Int. Ed. 48 (2009) 8952–8957.
[34] B.-D. Chang, I.B. Roninson, D. Porter, CDKI Pathway Inhibitors and Uses Thereof, 2009, US20090281129.
[35] D.C. Porter, I.B. Roninson, M.P. Wentland, CDKI Pathway Inhibitors and Uses Thereof, 2012, US20120071477.
[36] T. Dale, P.A. Clarke, C. Esdar, D. Waalboer, O. Adeniji-Popoola, M.-J. Ortiz-Ruiz, A. Mallinger, R.S. Samant, P. Czodrowski, D. Musil, D. Schwarz, K. Schneider, M. Stubbs, K. Ewan, E. Fraser, R. TePoele, W. Court, G. Box, M. Valenti, A. de Haven Brandon, S. Gowan, F. Rohdich, F. Raynaud, R. Schneider, O. Poeschke, A. Blaukat, P. Workman, K. Schiemann, S.A. Eccles, D. Wienke, J. Blagg, A selective chemical probe for exploring the role of CDK8 and CDK19 in human disease, Nat. Chem. Biol. 11 (2015) 973–980.
[37] J.M. Hatcher, E.S. Wang, L. Johannessen, N. Kwiatkowski, T. Sim, N.S. Gray, Development of highly potent and selective steroidal inhibitors and degraders of CDK8, ACS Med. Chem. Lett. 9 (2018) 540–545.
[38] E. Solum, T.V. Hansen, R. Aesoy, L. Herfindal, New CDK8 inhibitors as potential anti-leukemic agents - design, synthesis and biological evaluation, Bioorg. Med. Chem. 28 (2020) 115461–115468.
[39] I.B. Ronnison, D.C. Porter, M.P. Wentland, CDK8-CDK19 Selective Inhibitors and Their Use in Anti-metastatic and Chemopreventative Methods for Cancer, 2014, US20140038958A1.
[40] D. Ma, X. Chen, X.B. Shen, L.Q. Sheng, X.H. Liu, Binding patterns and structure-activity relationship of CDK8 inhibitors, Bioorg. Chem. 96 (2020) 103624.
[41] X. Lv, Y. Tian, S. Li, K. Cheng, X. Huang, H. Kong, C. Liao, Z. Xie, Discovery and development of cyclin-dependent kinase 8 inhibitors, Curr. Med. Chem. 27 (2020) 5429–5443.
[42] M. Xi, T. Chen, C. Wu, X. Gao, Y. Wu, X. Luo, K. Du, L. Yu, T. Cai, R. Shen, H. Sun, CDK8 as a therapeutic target for cancers and recent developments in discovery of CDK8 inhibitors, Eur. J. Med. Chem. 164 (2019) 77–91.
[43] S. Wang, S.J. McClue, J.R. Ferguson, J.D. Hull, S. Stokes, S. Parsons, R. Westwood, P.M. Fischer, Synthesis and configuration of the cyclin-dependent kinase inhibitor roscovitine and its enantiomer, Tetrahedron Asymmetry 12 (2001) 2891–2894.
[44] S. Wang, C. Meades, G. Wood, A. Osnowski, S. Anderson, R. Yuill, M. Thomas, M. Mezna, W. Jackson, C. Midgley, G. Griffiths, I. Fleming, S. Green, I. McNae, S.Y. Wu, C. McInnes, D. Zheleva, M.D. Walkinshaw, P.M. Fischer, 2-Anilino-4-(thiazol-5-yl)pyrimidine CDK inhibitors: synthesis, SAR analysis, X-ray crystallography, and biological activity, J. Med. Chem. 47 (2004) 1662–1675.
[45] S. Wang, G. Wood, C. Meades, G. Griffiths, C. Midgley, I. McNae, C. McInnes, S. Anderson, W. Jackson, M. Mezna, R. Yuill, M. Walkinshaw, P.M. Fischer, Synthesis and biological activity of 2-anilino-4-(1H-pyrrol-3-yl) pyrimidine CDK inhibitors, Bioorg. Med. Chem. Lett 14 (2004) 4237–4240.
[46] S. Wang, G. Griffiths, C.A. Midgley, A.L. Barnett, M. Cooper, J. Grabarek, L. Ingram, W. Jackson, G. Kontopidis, S.J. McClue, C. McInnes, J. McLachlan, C. Meades, M. Mezna, I. Stuart, M.P. Thomas, D.I. Zheleva, D.P. Lane, R.C. Jackson, D.M. Glover, D.G. Blake, P.M. Fischer, Discovery and characterization of 2-anilino-4-(thiazol-5-yl)pyrimidine transcriptional CDK inhibitors as anticancer agents, Chem. Biol. 17 (2010) 1111–1121.
[47] X. Liu, F. Lam, S. Shi, P.M. Fischer, S. Wang, In vitro antitumor mechanism of a novel cyclin-dependent kinase inhibitor CDKI-83, Invest. N. Drugs 30 (2012) 889–897.
[48] X. Liu, S. Shi, F. Lam, C. Pepper, P.M. Fischer, S. Wang, CDKI-71, a novel CDK9 inhibitor, is preferentially cytotoxic to cancer cells compared to flavopiridol, Int. J. Canc. 130 (2012) 1216–1226.
[49] H. Shao, S. Shi, S. Huang, A.J. Hole, A.Y. Abbas, S. Baumli, X. Liu, F. Lam, D.W. Foley, P.M. Fischer, M. Noble, J.A. Endicott, C. Pepper, S. Wang, Substituted 4-(thiazol-5-yl)-2-(phenylamino)pyrimidines are highly active CDK9 inhibitors: synthesis, X-ray crystal structures, structure-activity relationship, and anticancer activities, J. Med. Chem. 56 (2013) 640–659.
[50] F. Lam, A.Y. Abbas, H. Shao, T. Teo, J. Adams, P. Li, T.D. Bradshaw, P.M. Fischer, E. Walsby, C. Pepper, Y. Chen, J. Ding, S. Wang, Targeting RNA transcription and translation in ovarian cancer cells with pharmacological inhibitor CDKI-73, Oncotarget 5 (2014) 7691–7704.
[51] S. Tadesse, M. Yu, L.B. Mekonnen, F. Lam, S. Islam, K. Tomusange, M.H. Rahaman, B. Noll, S.K. Basnet, T. Teo, H. Albrecht, R. Milne, S. Wang, Highly potent, selective, and orally bioavailable 4-thiazol-N-(pyridin-2-yl) pyrimidin-2-amine cyclin-dependent kinases 4 and 6 inhibitors as anticancer drug candidates: design, synthesis, and evaluation, J. Med. Chem. 60 (2017) 1892–1915.
[52] S. Tadesse, G. Zhu, L.B. Mekonnen, J.L. Lenjisa, M. Yu, M.P. Brown, S. Wang, A novel series of N-(pyridin-2-yl)-4-(thiazol-5-yl)pyrimidin-2-amines as highly potent CDK4/6 inhibitors, Future Med. Chem. 9 (2017) 1495–1506.
[53] S. Tadesse, L. Bantie, K. Tomusange, M. Yu, S. Islam, N. Bykovska, B. Noll, G. Zhu, P. Li, F. Lam, M. Kumarasiri, R. Milne, S. Wang, Discovery and pharmacological characterization of a novel series of highly selective inhibitors of cyclin-dependent kinases 4 and 6 as anticancer agents, Br. J. Pharmacol. 175 (2018) 2399–2413.
[54] N.Z. Khair, J.L. Lenjisa, S. Tadesse, M. Kumarasiri, S.K.C. Basnet, L.B. Mekonnen, M. Li, S. Diab, M.J. Sykes, H. Albrecht, R. Milne, S. Wang, Discovery of CDK5 inhibitors through structure-guided approach, ACS Med. Chem. Lett. 10 (2019) 786–791.
[55] M.H. Rahaman, F. Lam, L. Zhong, T. Teo, J. Adams, M. Yu, R.W. Milne, C. Pepper, N.A. Lokman, C. Ricciardelli, M.K. Oehler, S. Wang, Targeting CDK9 for treatment of colorectal cancer, Mol. Oncol. 13 (2019) 2178–2193.
[56] M.H. Rahaman, Y. Yu, L. Zhong, J. Adams, F. Lam, P. Li, B. Noll, R. Milne, J. Peng, S. Wang, CDKI-73: an orally bioavailable and highly efficacious CDK9 inhibitor against acute myeloid leukemia, Invest. N. Drugs 37 (2019) 625–635.
[57] M. Kumarasiri, T. Teo, M. Yu, S. Philip, S.K. Basnet, H. Albrecht, M.J. Sykes, P. Wang, S. Wang, In search of novel CDK8 inhibitors by virtual screening, J. Chem. Inf. Model. 57 (2017) 413–416.
[58] M. Yu, T. Teo, Y. Yang, M. Li, Y. Long, S. Philip, B. Noll, G.K. Heinemann, S. Diab, P. Eldi, L. Mekonnen, A.T. Anshabo, M.H. Rahaman, R. Milne, J.D. Hayball, S. Wang, Potent and orally bioavailable CDK8 inhibitors: design, synthesis, structure-activity relationship analysis and biological evaluation, Eur. J. Med. Chem. 214 (2021) 113248.
[59] R.A. Friesner, J.L. Banks, R.B. Murphy, T.A. Halgren, J.J. Klicic, D.T. Mainz, M.P. Repasky, E.H. Knoll, M. Shelley, J.K. Perry, D.E. Shaw, P. Francis, P.S. Shenkin, Glide: a new approach for rapid, accurate docking and scoring. 1. method and assessment of docking accuracy, J. Med. Chem. 47 (2004) 1739–1749.
[60] T.A. Halgren, R.B. Murphy, R.A. Friesner, H.S. Beard, L.L. Frye, W.T. Pollard, J.L. Banks, Glide: a new approach for rapid, accurate docking and scoring. 2. enrichment factors in database screening, J. Med. Chem. 47 (2004) 1750–1759.
[61] X. Han, M. Jiang, C. Zhou, Z. Zhou, Z. Xu, L. Wang, A.V. Mayweg, R. Niu, T.G. Jin,

S. Yang, Discovery of potent and selective CDK8 inhibitors through FBDD approach, Bioorg. Med. Chem. Lett 27 (2017) 4488–4492.
[62] F.F. Wagner, L. Benajiba, A.J. Campbell, M. Weïwer, J.R. Sacher, J.P. Gale, L. Ross, A. Puissant, G. Alexe, A. Conway, M. Back, Y. Pikman, I. Galinsky, D.J. DeAngelo, R.M. Stone, T. Kaya, X. Shi, M.B. Robers, T. Machleidt, J. Wilkinson, O. Hermine, A. Kung, A.J. Stein, D. Lakshminarasimhan, M.T. Hemann, E. Scolnick, Y.-L. Zhang, J.Q. Pan, K. Stegmaier, E.B. Holson, Exploiting an Asp-Glu "switch" in glycogen synthase kinase 3 to design paralog-selective inhibitors for use in acute myeloid leukemia, Sci. Transl. Med. 10 (2018), eaam8460.
[63] T. Furuya, J.E.M.N. Klein, T. Ritter, Carbon-fluorine bond formation for the synthesis of aryl fluorides, Synthesis 2010 (2010) 1804–1821.
[64] M. Yu, P. Li, S.K. Basnet, M. Kumarasiri, S. Diab, T. Teo, H. Albrecht, S. Wang, Discovery of 4-(dihydropyridinon-3-yl)amino-5-methylthieno[2,3-d]pyrimidine derivatives as potent Mnk inhibitors: synthesis, structure-activity relationship analysis and biological evaluation, Eur. J. Med. Chem. 95 (2015) 116–126.
[65] R.K. Raju, J.W.G. Bloom, Y. An, S.E. Wheeler, Substituent effects on non-covalent interactions with aromatic rings: insights from computational chemistry, ChemPhysChem 12 (2011) 3116–3130.
[66] N.F. Smith, F.I. Raynaud, P. Workman, The application of cassette dosing for pharmacokinetic screening in small-molecule cancer drug discovery, Mol. Canc. Therapeut. 6 (2007) 428–440.
[67] L. Di, E.H. Kerns, Profiling drug-like properties in discovery research, Curr. Opin. Chem. Biol. 7 (2003) 402–408.
[68] E.N. Marieb, K. Hoehn, Human Anatomy & Physiology, Pearson Education, 2018.
[69] R. Roskoski Jr., The role of small molecule Flt3 receptor protein-tyrosine kinase inhibitors in the treatment of Flt3-positive acute myelogenous leukemias, Pharmacol. Res. 155 (2020) 104725.
[70] M. Yu, S. Tadesse, S. Wang, USFDA-approved small-molecule kinase inhibitors for cancer therapy, in: D.J. Abraham (Ed.) Burger's Medicinal Chemistry, Drug Discovery and Development (eighth ed.), John Wiley and Sons Ltd., Hoboken, in press.
[71] A. Kumari, O. Silakari, R.K. Singh, Recent advances in colony stimulating factor-1 receptor/c-FMS as an emerging target for various therapeutic implications, Biomed. Pharmacother. 103 (2018) 662–679.
[72] M.A. Cannarile, M. Weisser, W. Jacob, A.M. Jegg, C.H. Ries, D. Rüttinger, Colony-stimulating factor 1 receptor (CSF1R) inhibitors in cancer therapy, J. Immunother. Canc. 5 (2017). Article number: 53.
[73] E.R. Parrilla Castellar, J.K. Plichta, R. Davis, C. Gonzalez-Hunt, L.H. Sanders, Somatic mutations in LRRK2 identify a subset of invasive mammary carcinomas associated with high mutation burden, Am. J. Pathol. 190 (2020) 2478–2482.
[74] G. Lopez, G. Lazzeri, A. Rappa, G. Isimbaldi, F.M. Cribiù, E. Guerini-Rocco, S. Ferrero, V. Vaira, A. Di Fonzo, Comprehensive genomic analysis reveals the prognostic role of LRRK2 copy-number variations in human malignancies, Genes 11 (2020) 846.
[75] K. Jung, J.S. Choi, B.M. Koo, Y.J. Kim, J.Y. Song, M. Sung, E.S. Chang, K.W. Noh, S. An, M.S. Lee, K. Song, H. Lee, R.N. Kim, Y.K. Shin, D.Y. Oh, Y.L. Choi, TM4SF4 and LRRK2 are potential therapeutic targets in lung and breast cancers through outlier analysis, Canc. Res. Treat. 53 (2020) 9–24.
[76] R.S. Obach, R.L. Walsky, K. Venkatakrishnan, E.A. Gaman, J.B. Houston, L.M. Tremaine, The utility of in vitro cytochrome P450 inhibition data in the prediction of drug-drug interactions, J. Pharmacol. Exp. Therapeut. 316 (2006) 336–348.
[77] W. Haverkamp, G. Breithardt, A.J. Camm, M.J. Janse, M.R. Rosen, C. Antzelevitch, D. Escande, M. Franz, M. Malik, A. Moss, R. Shah, The potential for QT prolongation and proarrhythmia by non-antiarrhythmic drugs: clinical and regulatory implications. Report on a policy conference of the European Society of Cardiology, Eur. Heart J. 21 (2000) 1216–1231.
[78] J.M. Spear, Z. Lu, W.A. Russu, Pharmacological inhibition of CDK8 in triple-negative breast cancer cell line MDA-MB-468 increases E2F1 protein, induces phosphorylation of STAT3 and apoptosis, Molecules 25 (2020) 5728.
[79] E.M. Putz, D. Gotthardt, G. Hoermann, A. Csiszar, S. Wirth, A. Berger, E. Straka, D. Rigler, B. Wallner, A.M. Jamieson, W.F. Pickl, E.M. Zebedin-Brandl, M. Muller, T. Decker, V. Sexl, CDK8-mediated STAT1-S727 phosphorylation restrains NK cell cytotoxicity and tumor surveillance, Cell Rep. 4 (2013) 437–444.
[80] S. Elmore, Apoptosis: a review of programmed cell death, Toxicol. Pathol. 35 (2007) 495–516.
[81] J.I. Macdonald, F.A. Dick, Posttranslational modifications of the retinoblastoma tumor suppressor protein as determinants of function, Genes Canc. 3 (2012) 619–633.
[82] R.A. Friesner, R.B. Murphy, M.P. Repasky, L.L. Frye, J.R. Greenwood, T.A. Halgren, P.C. Sanschagrin, D.T. Mainz, Extra precision glide: docking and scoring incorporating a model of hydrophobic enclosure for protein-ligand complexes, J. Med. Chem. 49 (2006) 6177–6196.
[83] Y. Cheng, W.H. Prusoff, Relationship between the inhibition constant (KI) and the concentration of inhibitor which causes 50 per cent inhibition (I50) of an enzymatic reaction, Biochem. Pharmacol. 22 (1973) 3099–3108.
[84] L. Nikfarjam, P. Farzaneh, Prevention and detection of Mycoplasma contamination in cell culture, Cell J 13 (2012) 203–212.
[85] T. Teo, M. Yu, Y. Yang, T. Gillam, F. Lam, M.J. Sykes, S. Wang, Pharmacologic co-inhibition of Mnks and mTORC1 synergistically suppresses proliferation and perturbs cell cycle progression in blast crisis-chronic myeloid leukemia cells, Canc. Lett. 357 (2015) 612–623.
[86] S. Diab, T. Teo, M. Kumarasiri, P. Li, M. Yu, F. Lam, S.K. Basnet, M.J. Sykes, H. Albrecht, R. Milne, S. Wang, Discovery of 5-(2-(phenylamino)pyrimidin-4-yl)thiazol-2(3H)-one derivatives as potent Mnk2 inhibitors: synthesis, SAR analysis and biological evaluation, ChemMedChem 9 (2014) 962–972.